Combustion, Explosion, and Shock Waves, Vol. 46, No. 3, pp. –, 2010

Combustion of Heterogeneous Nanostructural Systems (Review)

A. S. Rogachev[1] and A. S. Mukasyan[2]

UDC 536.46

Translated from *Fizika Goreniya i Vzryva*, Vol. 46, No. 3, pp. 3–30, May–June, 2010.
Original article submitted June 9, 2009; revision submitted November 26, 2009.

The current status of research in the field of combustion of heterogeneous nanostructural systems is reviewed. Four classes of reactive media are considered: nanothermites, sol-gels, mechanically activated nanocomposites, and multilayer nanofilms. Based on the summary of publications, possible mechanisms of combustion in such systems and prospects of their further applications are discussed.

Key words: combustion, nanostructural systems, superthermites, sol-gel, solution combustion, mechanical activation, multilayer reactive nanofilms.

INTRODUCTION

Combustion investigations performed during the last decade discovered new classes of combustible systems, whose typical feature is the use of nano-sized reagents (fuel and oxidizer) and the associated extremely high reactivity, as compared to compositions with microscale heterogeneity. The present review deals with four classes of such systems: (i) reactive mixtures of metal and metal-oxide nanopowders, i.e., the so-called nanothermite compositions; (ii) sol-gel systems; (iii) nanocomposites obtained by mechanical activation of powder mixtures; (iv) multilayer reactive nanofilms. Investigations in each of these fields are performed almost independent of each other, and "cross references" are rather rare. Meanwhile, a comparison of specific features of combustion of these systems could be helpful in identifying the general laws and mechanisms of interactions in nanostructural combustible media, which one of the goals of this review. In addition, Russian publications do not provide adequate information about such systems: most publications were in foreign journals. Therefore, another objective of this paper is to attract attention of the Russian scientific community to this topic. We deliberately avoid the topic of combustion of nanopowder particles in gaseous oxidizers and their applications as additives to propellants and gunpowders, because this topic has been discussed in numerous publications, including monographs [1, 2].

Despite a comparatively short period of their research, the high-energy nanosystems considered find various applications: development of the new generation of energetic materials (nanothermites and mechanically activated compositions), synthesis of nanopowders including a wide range of catalysts (sol-gel systems), nanocrystalline materials with the microstructure optimized in advance (mechanically activated mixtures, and special types of welding/soldering of microelectronic components and other articles (multilayer reactive nanofilms). Therefore, a review of these new aspects is also of interest for practice.

POWDER NANOSYSTEMS

The development of production technologies of various nanopowders, including metals and their oxides, offers a possibility of preparing reactive heterogeneous compositions with nanostructural reagents. Though the range of available nanopowders is rather large (aluminum, boron, carbon, silicon, nickel, and many oxides), the review of publications shows that the main research objects were thermite nanosystems, which were called nanothermites or superthermites. These systems are highly exothermal mixtures of nanopowders of a reducing metal (A) and an oxide (BO_x) whose reaction releases a large amount of heat (Q) in the classical gross reaction of reduction

$$\mathrm{A} + \frac{y}{x}\mathrm{BO}_x = \frac{y}{x}\,\mathrm{B} + \mathrm{AO}_y + Q \qquad (1)$$

[1]Institute of Structural Macrokinetics and Material Science Problems, Russian Academy of Sciences, Chernogolovka 142432; rogachev@ism.ac.ru.
[2]Department of Chemical and Biomolecular Engineering, Notre Dame University, Notre Dame 46556, USA.

TABLE 1

Some Characteristics of Nanothermite Systems

System	ϕ	Metal particle size, nm	Oxide particle size	Reference
Al—MoO_3	0.5–4.5	17, 25, 30, 40, 53, 76, 100, 108, 160, 200	10 μ (plates 10 nm thick)	[5, 6]
	1.2	50, 80, 120	10 μm – 10 nm	[7]
	1–1.45	44, 80, 120	1 μm – 20 nm	[8]
	1	44	15.5 nm	[9]
	1.2–1.4	30, 45, 140, 170	BET = 66 m^2/g	[10]
	0.65–1.6	80	200 – 30 nm	[11]
Al—WO_3	1–1.5	80	100 – 20 nm	[12]
Al—Bi_2O_3	1–1.5	80	25 – 2 μm (filaments)	[13]
	1	40, 100	40, 108, 321, 416 mn	[12]
Al—CuO	1–1.5	80	100 – 20 mn	[12]
Al—Fe_2O_3	0.9–4	52	BET = 50 – 300 m^2/g	[14]

with formation of a more stable oxide (AO_y) and metal (B). In general practice, aluminum and magnesium are the most frequently used reducing metals, through nanoaluminum was mainly used for superthermites. The latest achievements in nanoaluminum production were described in recent monographs [2, 3].

Despite wide availability of nanopowders, preparing reactive mixtures involves several specific problems, including difficulties in homogeneous mixing of fine species, ageing (passivation) of nanopowders during their storage, and abnormally high sensitivity of nanoheterogeneous compositions to ignition and self-ignition. Optimal methods of storage and treatment of metal nanopowders are important not only from the viewpoint of safety, but also from the viewpoint of reliability and credibility of scientific data obtained [4]. Metal nanopowders with a large specific surface are prone to rapid oxidation in an oxygen-containing medium, which alters the reactivity of these powders (ageing). For this reason, the use of the same initial nanopowders, which were stored and mixed under different conditions, usually yields different results in terms of ignition and combustion characteristics of such systems. The data on the chemical compositions and particle sizes of reagents of some superthermite systems studied in [5–14] are summarized in Table 1. The widest range of metal nanoparticles was provided in experiments with the Al–MoO_3 system. The parameter ϕ, which determines the composition of the initial mixtures, is the ratio $\phi = (m_f/m_{ox})^{exp}/(m_f/m_{ox})^{st}$, where $(m_f/m_{ox})^{st}$ is the stoichiometric ratio of the fuel and oxidizer masses, and $(m_f/m_{ox})^{exp}$ is the ratio of the reagent masses used in experiments.

The parameters usually measured in the reported works were the parameters of initiation (ignition delay and temperature) and combustion (burning rate and temperature profiles) in these systems. The burning rate was determined in three different variants: (a) for freely standing pressed samples, (b) for loose mixtures on an open plane or in a channel open over its entire length, and (c) for loose mixtures in tubes open on one end. The process of ignition and combustion was most often registered by photodetectors or by high-speed video cameras (e.g., Phantom). Figure 1a shows the generalized data [8–10, 12, 14] on the burning rate U of nanothermites in closed channels or tubes, with the mixture density close to the loose density. Though the data are distributed in a wide range (from several hundreds of meters to one kilometer per second), these values are still much higher than the mean burning rates of heterogeneous systems with micron-size particles. To understand these results, we have to consider the specific features of experiments with combustion of nanothermite compositions in more detail.

The processes of combustion in the nanosystem consisting of aluminum and molybdenum oxide were studied in many works [5–12]. One of the first investigations of initiation and combustion of MoO_3–Al heterogeneous nanothermites was performed with pressed cylindrical samples (6 mm in diameter and 3 mm long) and revealed many specific features and difficulties in studying such objects [5]. Molybdenum oxide particles (MoO_3) ≈10 μm in diameter and 10 nm thick with plate-type morphology and a wide range of spherical particles of aluminum (Technanogy, Irvin, CA, USA) with the mean particle size from 15 nm to 20 μm were

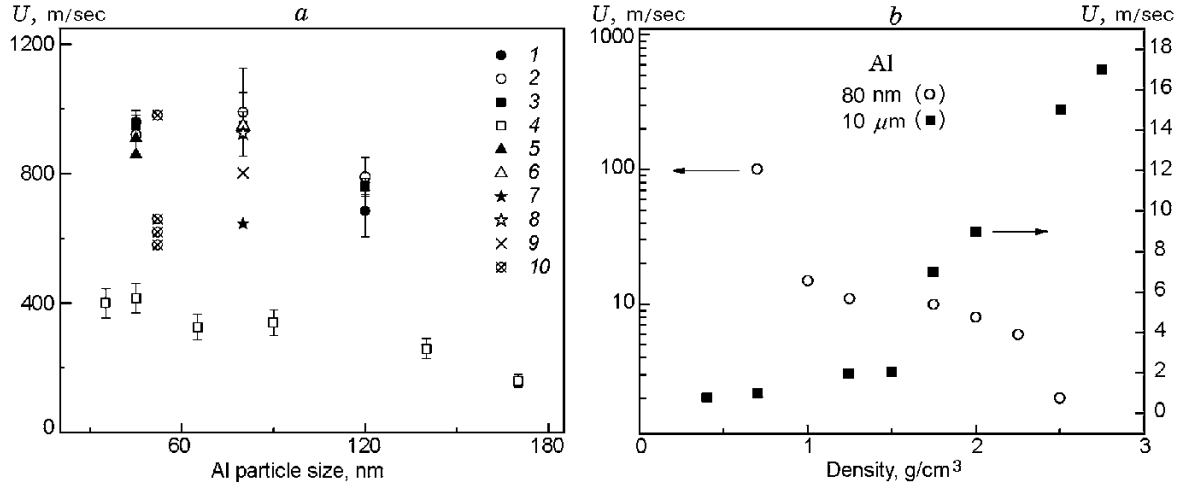

Fig. 1. Summary of the burning rates of Al–Me_2O_3 nanosystems in closed channels or tubes with low relative densities of the mixture (a) and burning rate of the MoO_3/Al thermite versus the density of the reactive medium for nano- and microheterogeneous mixtures [5] (b): MoO_3/Al [8] (1–3), MoO_3/Al [10] (4), MoO_3/Al [9] (5), MoO_3/Al [12] (6), Bi_2O_3/Al [12] (7), WO_3/Al [12] (8), CuO/Al [12] (9), and Fe_2O_3/Al [14] (10).

used (see Table 1). The problem of homogeneous mixing of nanopowders was solved by wet ultrasonic stirring in a hexane solution during 30 minutes. Granier and Pantoya [5] noted that, apparently, they could not ensure desired homogeneity for all compositions. It turned out that the compaction rate of nanoaluminum powder mixtures is rather low, and the relative density ensured by cold pressing was only 38% of the theoretical value, which is close to the loose density of micro-sized mixtures. The latter circumstance makes direct comparisons of results for nano- and microheterogeneous compositions rather difficult. One more specific feature is associated with a strong influence of oxide films on the properties of metal nanoparticles. The fraction of active aluminum decreases from 97.5% for 20-μm particles to 44% for 30-nm particles. This effect not only hinders precise determination of the amount of metal aluminum in the initial composition, but can also alter the reaction mechanism owing to reduction of the adiabatic burning temperature. In addition, in view of the high porosity of the samples, experiments should be performed in an inert medium rather than in air, as it was done in [5–8, 10–13]. It is difficult to interpret results because of competing reactions of solid reagents with each other and with the ambient gases (oxygen, nitrogen). Nevertheless, the measured burning rates for pressed samples were within 10 m/sec, which is lower than those plotted in Fig. 1a by one or two orders of magnitude.

Bockmom et al. [8] used substantially longer samples (about 10 cm with a diameter of 2 mm) to study the dependence of the burning rate on the metal particle size (Al powders with 45, 80, and 120 nm). In all experiments, powders with a loose density (relative density equal to 5–10% of the theoretical value) were placed into long acrylic tubes and were ignited from the closed end; the second end of the tube was left open. The burning rate was estimated on the basis of the frame-by-frame analysis of high-speed video recording of the process and measurements of changes in the gas pressure along the tube after reaction initiation. Extremely high burning rates were obtained (600–1000 m/sec), which exceed those given for the same compositions in [5, 6] by a factor of hundreds. Though such burning rates offer many prospects in constructing hypotheses on combustion mechanisms, the primary necessary is to analyze the test conditions and verification of the adequacy of the results obtained.

First, it was noted that the entire reactive medium was "blown off" from the acrylic tube and it was impossible to analyze the composition and morphology of the products after combustion. Second, in this arrangement of experiments, the high (up to 100 atm) measured pressures of the gas (of an unknown nature: gasification of the reagents or desorption of foreign gases?) in the front really indicate that the loose powder could be blown off from the channel. It is not clear what was measured: the velocity of the combustion wave in the heterogeneous aluminum–molybdenum oxide system or the velocity of exhaustion of the heated gas from the tube after reaction initiation. If the latter case was realized, then, most probably, no conclusions about the reaction mechanism in the system can be drawn. Un-

derstanding the role of the gas-phase component in the process observed, Bockmom et al. [8] proposed a convective mechanism of combustion, based on transportation of melted Al and gasified MoO_3 by the gas flow to the zone of non-reacted products.

This mechanism actually agrees with the previous conclusion based on the analysis of model experiments [9]. The original (so-called "barrier") experiments with sapphire disks (0.4 mm thick and 4.4 mm in diameter) placed on the way of combustion wave propagation, the measurements of the pressure wave profile, and the results on combustion in vacuum should be noted. All these experiments were performed with loose mixtures of Al (44 nm) and MoO_3 (15 nm) nanopowders placed into long acrylic tubes. Transparent disks for radiative heat transfer were demonstrated to stop the combustion wave front. At the same time, the front jumped through inert loose-density plugs made of oxide powders (several millimeters thick). The results of pressure measurements at the open end of the tube showed that the main increase in pressure was observed ahead of the luminescent front, at a distance of ≈7 mm from the latter, the pressure reached the maximum value (≈250 atm) during the time of 10–12 μsec, and the velocity of the luminescent front was ≈900 m/sec. Based on these measurements, the authors estimated the width of the "ignition" zone (apparently, they meant the total thickness of the heating and combustion zones) to be 10 mm. If this is the case, then the rough estimate of the characteristic reaction time is 1 μsec.

Son et al. [11] studied combustion in even thinner microchannels (inner diameter 0.48, 1.01, and 1.85 mm). Consecutive frames of the process are shown in Fig. 2a. As in [8], extremely high burning rates (400–1000 m/sec) were registered, despite the small diameters of the samples. The burning rate decreased with decreasing channel diameter (Fig. 2b), which was attributed to higher heat losses. Though the main result of that paper was demonstration of the possibility of superthermite combustion in slender channels, the proposed mechanism of combustion should also be noted. The mechanism does not differ much from that considered in earlier papers [8, 9] and is based on the leading role of the hot gas (in the case considered, sublimated aluminum oxide), which "pushes" the melted molybdenum to the non-reacted medium, which leads to rapid heating and reaction of the latter. The model is based only on the results of thermodynamic calculations, which predict extremely high adiabatic temperatures of combustion (above 2900 K, i.e., above the temperatures of aluminum oxide sublimation and molybdenum melting). Obviously, it is necessary to measure the temperature profiles of fast processes with a time resolution of $\leqslant 1$ μsec to verify the mechanism.

Walter et al. [10] discussed an important problem of production and storage of nanopowders. It was emphasized that the work with superthermite mixtures should be performed in accordance with the most rigorous safety requirements. The influence of the time and conditions of storage of nanopowders (by an example of Al and MoO_3) on their chemical composition and,hence, on the reactivity was demonstrated. In particular, a parabolic law of oxide film growth on Al particles being stored in a glass desiccator under non-sealed conditions was obtained. Under such storage conditions, the molybdenum oxide powder loses up to one half of its Brunauer–Emmett–Teller (BET) specific surface during ten days. It should also be noted that the large time-dependent content of oxide phases makes the exact estimate of the ratio of reagents in superthermite systems rather difficult. For this reason, in turn, there are problems in comparisons of results obtained in different works. In particular, the measured burning rates for loose powders in the MoO_3–Al system [10] were in the range from 350 to 400 m/sec, which is substantially lower than the values of 600 to 1000 m/sec obtained during combustion of the same compositions in acrylic tubes.

Sanders et al. [12] studied the burning rate as a function of the composition and density of the reactive mixture for four thermite systems: Al/WO_3, Al/MoO_3, Al/Bi_2O_3, and Al/CuO. In all cases, the Al powder with a particle size of 80 nm was used, whereas the oxide powders were different: WO_3 (100×20 nm) and MoO_3 (200×30 nm) flakes, CuO (20×100 nm) nanocolumns, and micron-sized (2 μm) Bi_2O_3 particles. In the latter case, coarser particles were used because of the high sensitivity of nanomixtures containing bismuth oxide to ignition (see also [13]). Combustion of these compositions was studied in three different situations: in a closed reactor (the dynamics of pressure was measured), on an open substrate (loose density), and in long thin (≈3.5 mm) acrylic tubes closed on one end (with the relative loose density of 47%). As in the previous works, the wave front propagation velocity was measured by photodetectors and pressure sensors. In our opinion, two basic results should be noted. First, the burning rate for all compositions on the substrate turned out to be substantially lower than for those in the tube: 365/925 m/sec for WO_3, 320/950 m/sec for MoO_3, 525/800 m/sec for CuO, and 425/645 m/sec for Bi_2O_3. Second, the burning rate of the packed mixtures in acrylic tubes was much lower than that in loose mixtures: 580/950 m/sec for MoO_3 and 560/645 m/sec for Bi_2O_3. The maximum pressures of the gas for MoO_3-based compositions having a higher density are higher

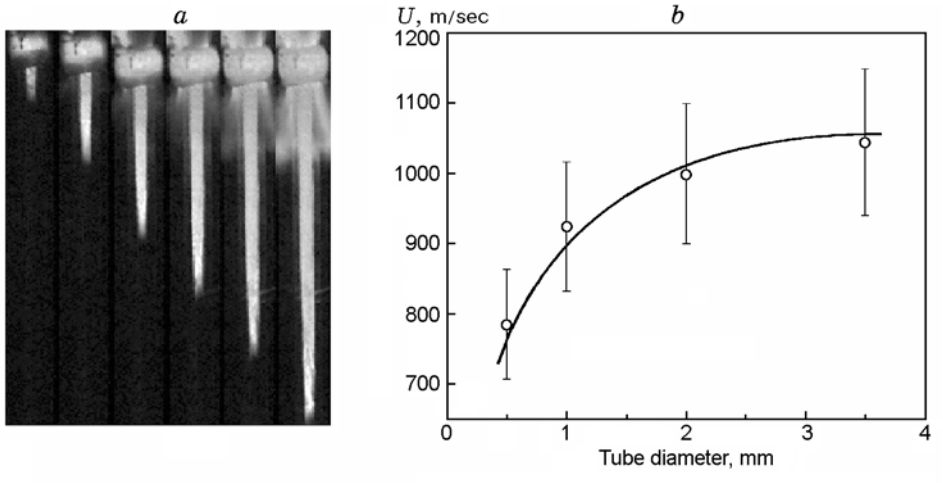

Fig. 2. Consecutive frames (with an interval of 13.8 μsec) of combustion in an acrylic tube (inner diameter 2 mm) (a) and burning rate as a function of the tube diameter (b) (based on results of [11]).

than that for loose mixtures (455/185 atm), whereas the corresponding value for Bi_2O_3 is lower (395/535 atm). These results confirm the strong effect of the gas phase on the measured displacement of the luminescent front. At the same time, it is not clear (a) what is the composition of the gas phase: sublimated initial components, combustion products, or gasified admixtures from the nanopowder surface, and (b) whether the location of the luminescent front coincides with the real front of the chemical reaction determining the velocity of the combustion process. Without answers to these questions, all attempts to explain the superthermite combustion mechanism are non-proved hypothesis.

An important point in discussing the problem is the result of Pantoya and Granier [6] who compared the burning rates as functions of the reactive medium density in the MoO_3–Al system for nano- and micro-heterogeneous mixtures (see Fig. 1b). It was shown that the burning rate in micron-sized powders increases with increasing density of the reactive medium (which is associated with the increase in thermal diffusivity of the mixture). The opposite effect was found in nanomixtures: very high burning rates (≈1000 m/sec) for samples with a comparatively low density and moderate burning rates (≈1 m/sec) for dense samples, which is commensurable to data obtained for micron-sized powders. These results indicate that the extremely high velocities of luminescent front propagation during combustion of superthermites in slender channels are caused by the macrokinetics of exhaustion of hot gases in slender channels rather than by the kinetics of chemical reactions in nanosystems. Therefore, the question about significant differences (two or three orders) in the reaction kinetics of nano- and microsystems remains open.

Nevertheless, nanosystems are undoubtedly more "reactive" than compositions with micro-scale heterogeneity. As is seen from thermocouple measurements, the ignition delay and for the nanothermite and its ignition temperature are much lower than the corresponding values for the mixture of a similar composition prepared from micron-sized powders (Fig. 3), even though a less powerful heat source was used to ignite the nanosystem [5]. Under identical ignition conditions (the radiation of a 50-W CO_2 laser is focused into a beam 2 mm in diameter on the flat end surface of a cylindrical sample), a nanothermite with particles ranging from 17 to 200 nm is ignited approximately within 20 msec, and this ignition time depends only weakly on the particle size. For a thermite of a similar composition with micron-sized particles (3.5–20 μm), ignition under the same conditions requires 1–5 sec, and this time increases with increasing particle size.

The results of the differential thermal analysis (DTA) confirm that the temperature needed for the reaction to begin in nanothermite systems is lower. For instance, the main exothermal peak appears in the MoO_3–Al system at a temperature of ≈950 °C if the Al particle size is 10 μm and ≈500 °C if the Al particle size is 40 nm [6]. Certainly, these values differ significantly from the results of thermocouple measurements in the course of ignition of the samples (see Fig. 3), but the qualitative conclusion is the same: micron-sized powders exhibit intense interaction when the melting point of aluminum is reached, whereas nanopowders are fairly active in solid-phase reactions as well. Pantoya and Granier also studied this problem by means of DTA for different heating rates [7].An approximately linear dependence of the temperature of the reaction begin-

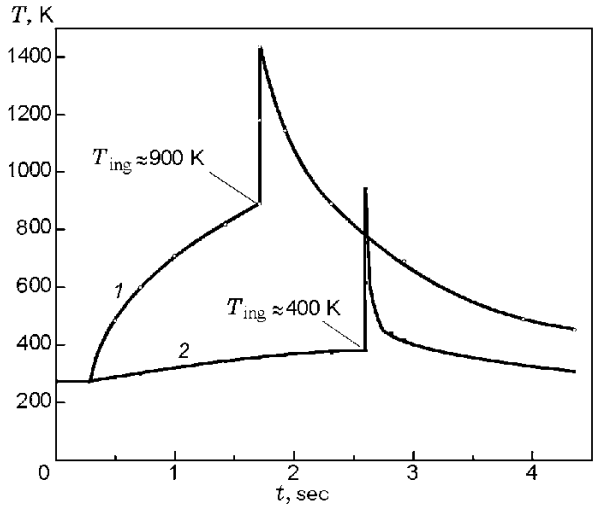

Fig. 3. Temperature curves (measurements by a C-type thermocouple 75 μm thick on the pellet surface) of heating and ignition of the Al–MoO_3 thermite with the aluminum particle size of 3–4 μm (curve 1) and 55 nm (curve 2). The mixture is ignited by laser radiation with a power of 15 (1) and 5 W (2) (based on results of [5]).

ning on the particle size and a weak dependence of this characteristic on the heating rate were demonstrated.

Puszinski et al. [13] studied the parameters of initiation and combustion in a Bi_2O_3/Al nanothermite system. Particular attention was paid to searching for effective inhibitors that would allow mixing of aluminum and bismuth oxide in water without significant changes in the chemical composition of the reactive mixture. In particular, it was shown that the ammonia dihydrophosphate ($NH_4H_2PO_4$) is the best inhibitor: forming a coating on the aluminum nanoparticle surface, it allow mixing of Al and Bi_2O_3 powders in water and obtaining mixtures with a highly homogeneous composition. In addition, the problem of the electrostatic charge accumulated on the surface of nanopowder particles during its mixing, for instance, in a glass vial was studied in detail. The sensitivity of superthermite system in terms of ignition under the action of an electrostatic discharge was examined. The aluminum–bismuth oxide system was demonstrated to be the most sensitive one, because its ignition requires only $\approx$0.1 μJ of energy (the corresponding values for Al–MoO_3 and Al–Fe_2O_3 systems are $\approx$50 μJ and $\approx$1 μJ, respectively). The use of such an inhibitor as oleic acid leads to a significant (by more than an order of magnitude) increase in energy necessary for self-ignition of the system under the same conditions. This study again illustrates the importance of safety aspects in operations with nanopowders.

The classical iron oxide–aluminum thermite system was studied in [13–16]. Plantier et al. [14] investigated combustion of this mixture in an open (0.3×0.3 cm channel 5 cm long) and closed (tubes 0.3 and 0.6 cm in diameter, 10 cm long) variants for different iron oxide powders (with a specific surface of 50–300 m^2/g). The measured range of the burning rates for the open channel was rather wide (0.02–120 m/sec) and depended on the morphology and phase composition of the iron nanopowder. The burning rates in experiments with a tube closed on one end were fairly high (up to 950 m/sec). The burning rates for all compositions were higher than those in experiments with the open channel experiments.

Mehendale et al. [15] studied the combustion of an Al–Fe_2O_3 system with the α-phase Fe_2O_3 powder was obtained by the method of iron hydroxide annealing. Addition of various surfactants was used to modify the iron oxide powder microstructure (mainly, the pore size and distribution). The burning rates in the open channel varied from 7 to 15 m/sec without addition of surfactants and up to 19 m/sec with addition of surfactants. A similar pattern was observed in the tubes: $\approx$150 and 270 m/sec, respectively. The authors attributed the increase in the burning rate to the increase in the contact area between the reagents in more ordered and finer structures of powders obtained with addition of surfactants. Prakash et al. [16] applied the sol-gel method (the reagents were $FeCl_3 \cdot 6H_2O$ and 1,2-epoxybutane) for obtaining the fine-grain ($\approx$100 nm) iron oxide powder. The mixture of this powder with the aluminum powder (40 nm) obtained by simple mixing in the ethanol environment burned at approximately 4 m/sec.

Finally, we should note the paper of Perry et al. [17] who studied the combustion of the Al/WO_3 nanosystem The Al powder (Nanotechnologies Inc., Austin, TX) with a particle size of $\approx$40 nm was mixed with the tungsten oxide powder obtained by the method of deposition in chemical solutions and having a plate-type morphology with a particle size of 100×7 nm. The burning rate for a stoichiometric composition with a loose density on the open substrate was $\approx$250 m/sec.

Based on the above-described results, we can draw some preliminary conclusions on combustion of heterogeneous nanosystems. These conclusions can be classified into two groups. The first group covers the aspects of nanopowder synthesis, preparation of high-energy mixtures, and experimental techniques associated with the characteristic scales of the proces sunder study. The second group refers to the fundamental nature of combustion of such systems and possible mechanisms of interaction.

The range of available non-oxide nanopowders is not too large (Al, Ni, Fe, and Si). At the moment only nanoaluminum powders have been synthesized in a wide range of particle sizes, starting from ≈20 nm. At the same time, various nano-sized powders of metal oxides are easily available. Because of the high reactivity of metal nanoparticles, particular attention should be paid to problems of storage and preparation of samples. These issues are important not only from the view of safety engineering, but also for adequate arrangement of basic research. The effect of oxide films on the metal particle surface, which can occupy a considerable part of the volume of nanoparticles, on the mechanism of combustion of "gasless" systems has not been studied.

The above-considered reactive nanosystems are characterized by low ignition temperatures and short ignition delays, as compared with their microheterogeneous analogs. These effects would have been obvious if the temperatures observed were not so low. Indeed, experimental data show that, possibly, purely solid-phase reactions are responsible for system self-ignition. Studying the kinetics of solid-phase reactions in nanosystems is a new field of science. The range of the burning rates in such systems is even more surprising. Different authors give the combustion wave velocities (>1000 m/sec) at the level of the velocity of sound in the reactive medium, emphasizing the absence of detonation. In our opinion, these data require both experimental validation and, possibly, revision of the interpretation of the results obtained. In any case, investigations of the combustion of nanosystems requires new methods of measuring combustion parameters in heterogeneous systems with time scales of $\leqslant 1$ μsec and heterogeneity scales of $\leqslant 0.1$ μm.

SOL-GEL SYSTEMS

The second class of combustible systems, which refer to nanosystems, include gels obtained by drying water-based reactive solutions. The sol-gel process has been mainly studied as a method for production of nanopowders [18–20], which can be used, for instance, for preparing superthermite mixtures [16]. Reagents are dissolved in water, and their molecular-level mixing naturally occurs. After that, the solvent (e.g., water) is removed by drying extraction; in some systems, gelatinization occurs: first, a colloid suspension is formed, then, mechanical contact arise between the colloid particles, grids composed of colloid particles appear, and the medium viscosity drastically increases: a gel is formed. Depending on the regime of solvent removal, it is possible to obtain an extremely porous aerogel (with a porosity greater than 95%) or a comparatively dense, almost pore-free xerogel. In any case, the gel consists of nanosized particles, and this is the difference of the sol-gel-process from the conventional procedure of crystallization of a solid substance from a solution.

Let us discuss the process of direct (one-stage) formation of reaction-capable gels from water-based solutions of metal nitrates and a combustible substance (glycine, carbamide, hydrazine, etc.) and the specific features of their combustion. This method was called the "solution combustion." Let us consider this process by an example of combustion of an iron-containing system with the only final solid-phase product being the iron oxide. Iron oxide, which is a known pigment with a large specific surface and the particle size down to 3 nm, is obtained by an industrial method of deposition from solutions [21]. This process takes a rather long time (hours) and is performed at low temperatures (≈400 K). Another method is the combustion of the metal powder in a gas (oxygen or air) [22]. This is a fast (seconds) and high-temperature (>2300 K) process, but it provides comparatively coarse (tens of micrometers) particles. An attempt to unite these two approaches led to the idea of combustion of solutions and sol-gel systems.

The oxidizer can be iron nitrate $Fe(NO_3)_3 \cdot 9H_2O$, which contains several molecules of bound water. As was noted above, the spectrum of reducing agents is rather wide [19, 23], but here we will consider glycine $CH_2NH_2CO_2H$. Under standard conditions, both reagents are powders with melting points of 135 and 251 °C, respectively. It is important that both species are well soluble in water and form a homogeneous water solution.

The dependence of the adiabatic temperature of combustion in such a system on the ratio of the reagents and the amount of water is shown in Fig. 4 [27]. The gross reaction for combustion in air can be written in the form

$$\mathrm{Fe(NO_3)_3} + \frac{5}{3}\,\phi \mathrm{CH_2NH_2CO_2H} + \\ + \frac{15}{4}(\phi - 1)\mathrm{O_2} \Rightarrow \frac{1}{2}\,\mathrm{Fe_2O_3^{(s)}} + \frac{10}{3}\,\phi \mathrm{CO_2^{(g)}} + \\ + \frac{25}{6}\,\phi \mathrm{H_2O^{(g)}} + \frac{1}{2}\left(\frac{5}{3}\,\phi + 3\right)\mathrm{N_2^{(g)}},$$

where $\phi = 1$ corresponds to a stoichiometric composition, where the reaction proceeds completely without using oxygen contained in air; $\phi > 1$ (<1) refers to rich (lean) mixtures. It is seen from Fig. 4 that the system, first, is strongly isothermal: the adiabatic temperature of combustion for a stoichiometric composition in the absence of water is above 2200 K. Second, a large amount of gas-phase products is formed during combustion, which increases with increasing ϕ. Third, the

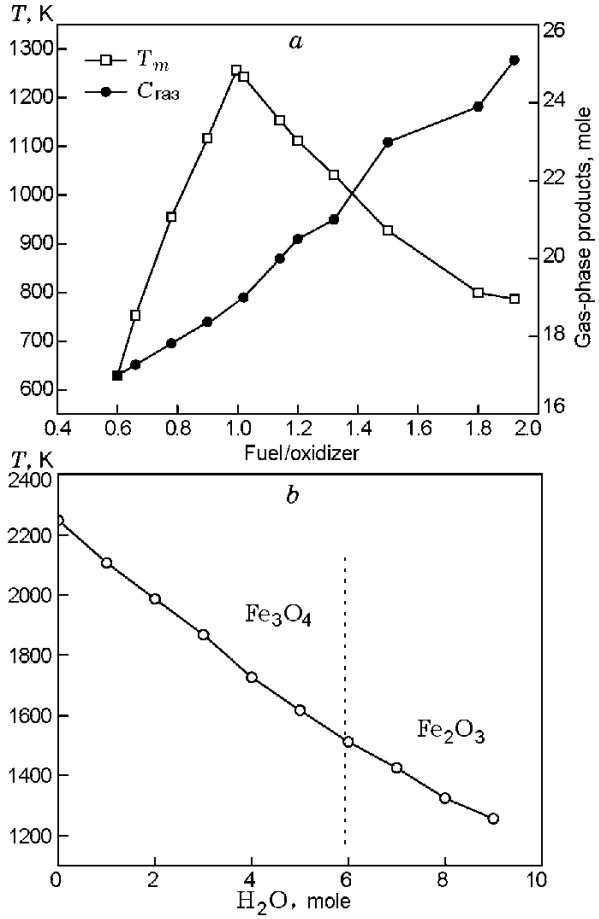

Fig. 4. Adiabatic temperature of combustion and amount of gas-phase products of combustion (thermodynamic calculation) in the glycine–iron nitrate system versus the equivalence ratio ϕ = fuel/oxidizer = $[C_2H_5NO_2]/[Fe(NO_3)_3 \cdot 9H_2O]$ (a) and versus the amount of residual water at $\phi = 1$ (b) (based on results of [27]).

amount of water in the system determines the phase composition of solid-phase products.

As in combustion of heterogeneous powder systems, two regimes of interactions are possible in sol-gel systems; volume thermal explosion and autowave propagation of the reaction [24, 25]. Various methods of heating the reactive medium up to the thermal explosion are used: heating on a usual laboratory oven, heating of the solution in an over with a given temperature, heating in microwave ovens, etc.

Figure 5 shows a typical thermogram of the process for the case of heating of the $Fe(NO_3)_3 \cdot 9H_2O$ + $C_2H_5NO_2$ solution by a heat source with a constant temperature. The process can be divided into several stages. As long as water is boiling at 100 °C, the temperature is constant, and the length of this zone de-

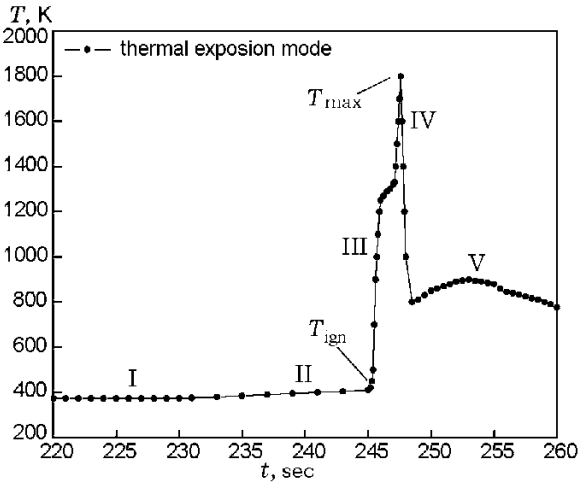

Fig. 5. Time evolution of the thermal explosion temperature in the $Fe(NO_3)_3 \cdot 9H_2O + C_2H_5NO_2$ system [27, 28].

pends on the amount of water in the initial solution and on the power of heating. When all free water boils away, there follows a short (several seconds) stage (II) of heating to the ignition temperature (T_{ign}). Note that the medium in this pre-explosion zone is a viscous homogeneous sol-gel mass whose crystalline structure has not yet been formed (the X-ray diffraction analysis does not reveal any peaks). The thermal explosion (III) occurs at T_{ign} = 400 K, and the temperature rapidly (≈1000 K/sec) increases to its maximum value. At the next stage (IV), the temperature decreases owing to intense gas release. After that, there follows a slow increase in temperature (stage V) owing to the oxidation reaction with participation of oxygen contained in air. As a result, a single-phase powder of iron nanooxide (Fe_2O_3) is obtained.

There are many publications on using the solution combustion as a method of synthesizing various nanopowders (see, e.g., the monograph [19] and the reviews [20, 26, 27]). The nano-scale size of combustion products and their high specific surface are caused by several reasons: (i) molecular level of mixing of reagents in the solution, which ensures an extremely small scale of heterogeneity of the initial sol-gels; (ii) large amount of gas-phase products whose intense liberation prevents agglomeration (sintering) of solid-phase products; (iii) specific features of formation of the solid-phase product in the form of thin layers or suspensions, which is responsible for the high rate of product cooling, i.e., short duration (<1 sec) of the high-temperature zone behind the combustion wave.

In this paper, however, we mainly consider the laws and mechanisms of the combustion process rather than

microstructural characteristics of materials obtained, and there are few publications on this topic. What is the factor responsible for the thermal explosion temperature in such a system? What is the mechanism of structural transformation from the sol-gel to the solid particle? What are the main parameters of the combustion wave? How do these parameters affect the properties of the synthesis product? How can the process be controlled? These and many other questions still wait for answers. Paying much attention to the material science aspects of the process and synthesis product properties, most researchers were little interested in the combustion mechanism proper. As the long-time experience of using combustion processes for obtaining various materials shows, it is impossible to develop effective technologies for production of materials without knowing the physical laws of the phenomenon. Let us consider the available publications.

Deshpande et al. [28] studied the mechanism of the thermal explosion in the iron nitrate–glycine system with the use of differential scanning calorimetry (DSC) and thermogravimetry (TG) It was demonstrated that the self-ignition temperature is practically independent of the ratio of reagents and on other parameters of the process, such as the volume of the reactive medium and the chemical nature of the ambient atmosphere (air or inert gas). The range of temperature where drastic enhancement of the reaction is observed coincides with temperatures of intense decomposition of iron nitrate (135–140 °C). It is known [29] that heating of $Fe(NO_3)_3 \cdot 2H_2O$ results hydrolysis with formation of HNO_3 molecules, which immediately react with glycine. Similarly, the ignition temperature in the iron nitrate–hydrazine (N_2H_4) system is equal to the boiling point of hydrazine (≈105 °C), which is lower than the temperature of nitrate decomposition. A hypothesis was put forward that the temperatures of self-ignition of such systems are related to the temperatures of phase transitions or decomposition of compounds (dissociation, evaporation, etc.). It is of interest that similar conclusions were made by the authors of many publications on the thermal explosion of heterogeneous powder systems (e.g., [30, 31]). Understanding of this face can substantially facilitate the control of this process, but the conclusion still needs comprehensive verifications. This and other aspects (role of inert dilutants critical scales, inhibitors and catalysis, closed and open volumes) associated with the thermal explosion in sol-gel-type media is a new area of the combustion science, which was not yet adequately studied.

As was noted above, the thermal explosion is the most "popular" mode for researchers, but it was also demonstrated in many papers that the combustion in the sol-gel system can also proceed in the autowave regime. Figure 6a shows a typical curve of propagation of the combustion wave front in the $Fe(NO_3)_3$ + $C_2H_5NO_2$ system heated to 373 K (below the temperature of self-ignition of this composition). Note that the maximum burning temperature in the front is substantially lower than in the case of the thermal explosion (see Fig. 5), which is, apparently, caused by a large amount of water still present in the reactive medium. The burning rate U is plotted in Fig. 6b as a function of the initial temperature T_0. Note that the range of the burning rates is 0.5–2.0 cm/sec, which is considerably higher than the burning rates of the superthermite systems considered above.Though the value of U increases with increasing T_0, as in conventional heterogeneous systems, the temperature coefficient of sensitivity of the burning rate is substantially higher for the solution combustion. Indeed, a typical value of $d(\ln U)/dT$ for powder mixtures is $\approx 10^{-3}$ cm $\cdot$ sec$^{-1} \cdot$ K^{-1}, whereas we have ≈0.05 cm $\cdot$ sec$^{-1} \cdot$ K^{-1} for the system considered, i.e., a minor change in T_0 leads to a strong change in the burning rate [24].

Available publications mainly describe the dependence of the properties of combustion products on various parameters, such as the ratio of the species [32–35], acidity (pH) of the reactive medium [36–38], and dilution of the reactive composition by solid-phase fine-grain powders [39–41]. Though it is difficult to find more or less systematized data on combustion parameters, some specific features can still be noted.

Wu et al. [36] studied the combustion in a system including a mixture of nitrates $Me^{\nu}(NO_3)_{\nu}$, where Me = Zn, Ni, or Fe, citric acid, and additives of an inert powder (silicon nanooxide). Nitrates of zinc, iron, and nickel with the ratio Ni : Zn : Fe = 1 : 1 : 4 were dissolved in deionized water with addition of 5 wt.% of the SiO_2 aerosol (<100 nm). The ratio between the nitrates and citric acid was 1 : 1. A small amount of ammonia was used to change the acidity of the reactive medium (in the pH range from 3 to 7), which did not affect the exothermal properties of the system. The entire mixture was stirred during 6 h at a temperature of 70 °C and then was dried in vacuum at 100 °C during 24 h. After that, the reaction was locally initiated, and the combustion wave front propagated over the gel with formation of a nanopowder having a complex composition. It turned out that the size of the product grains and crystallites, which was determined by the method of transmission electron microscopy (TEM) and on the basis of broadening of diffraction X-ray peaks, drastically decreased with decreasing pH (i.e., with increasing acidity of the medium) The DSC study of the reaction stages showed that the activation energy of the

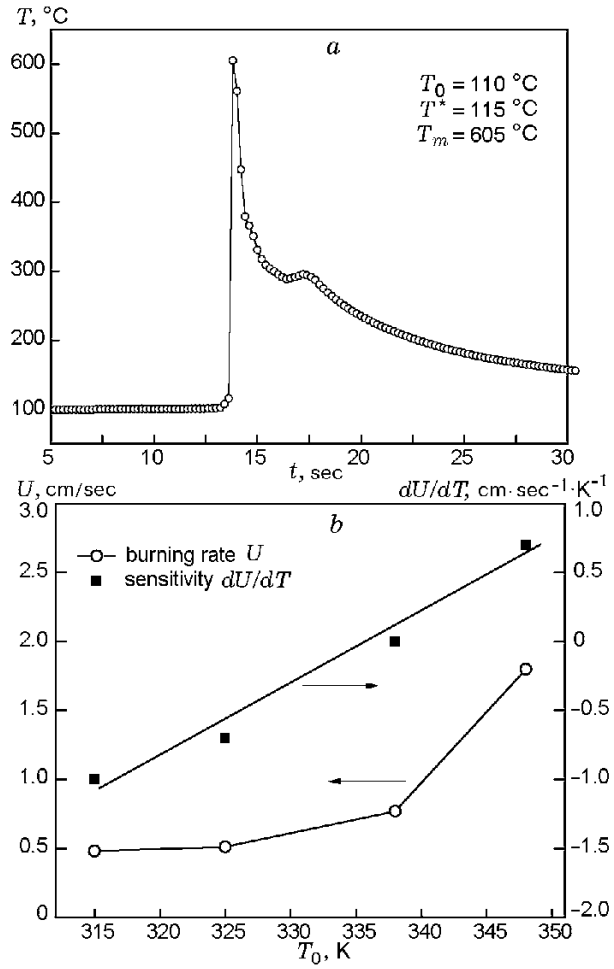

Fig. 6. Typical temperature profile of the combustion wave (a) and burning rate as a function of the initial temperature (b) in the glycine–iron nitrate system [27, 28].

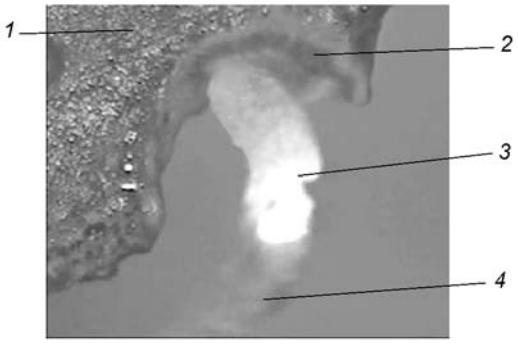

Fig. 7. Macrophotograph of the combustion wave in the glycine–iron nitrate sol-gel system [42]: 1) melting zone, 2) intermediate reaction with formation of a solid intermediate product, 3) basic reaction, and 4) final solid-phase product.

oxidation stage (formation of oxide nanopowders) decreases with decreasing pH of the initial solution: it is 633 kJ/mole in the neutral solution with pH= 7 and 536 kJ/mole at pH= 5 and drastically decreases to 55 kJ/mole at pH= 3. Obviously, the mechanism of the oxidation reaction becomes different. Wu et al. [36] attributed this fact to an increase in the concentration of NO_3 ions in the solution, which favor faster decomposition of organic substances at the stage of gel formation preceding the stage of oxidation with oxygen. In other words, the molecular composition and the structure of the gel at the beginning of the oxygen-assisted combustion reaction depend on the acidity of the initial water-based solution. There are no doubts that this effect requires further investigations.

The first activities on studying the combustion mechanism with the use of macroscopic video filming are of particular interest [25, 42]. It turned out that the combustion wave front, for instance, for the iron nitrate–glycine system, consists of many hot spots, which form the bases for growth of porous fine-grain iron oxide columns. The macrostructure of the combustion wave is shown in Fig. 7. It is seen that the process has many stages: it is possible to identify zones of melting and of the intermediate and basic reactions. The mechanism of formation of the crystalline solid phase from a sol-gel-type solution in the combustion mode is still poorly understood and is of great interest from the viewpoint of both basic research and applications.

To conclude, we can note an interesting type of combustion where the above-described solutions impregnate porous inert [25, 41, 43] and reactive [25, 44] media. It turned out that the combustion wave can be initiated in such systems as well. In the first case, catalysts on an inert support with a large specific surface and improved mechanical properties are obtained. Some data on the burning rate and temperature dependences in such systems can be found in [41]. In the case of an active porous medium, it is possible to realize the combustion process in weakly exothermal solutions [25] or continuous synthesis of nanopowders [44]. In terms of basic research, it is interesting to study (a) the combustion wave structure (reaction of the active substrate + the reaction of the solution) and (b) the transition from the readily controlled regime of smoldering to the convective combustion mode.

Summarizing the review on combustion of sol-gel systems, we should note that they have comparatively low temperatures of self-ignition, as well as superthermite nanomixtures. Another similar feature is the formation, in addition to the condensed phase, of a large

amount of gases in the combustion wave, which affect the formation of the microstructure of the solid-phase product.On the other hand, though the scale of heterogeneity of the initial sol-gel media is smaller than that in the mixtures of metal and oxide nanopowders (gel particles are smaller than the particles in superthermite mixtures), the burning rates of reactive sol-gels are substantially lower than the burning rates of powder mixtures. This can be attributed to the low thermal conductivity of gels. Finally, we should note that the mechanism of combustion in such systems is poorly studied, despite the great potential for various applications, basically related to synthesis of nanomaterials. One of the goals of the present review is to attract attention of researchers to this interesting phenomenon.

MECHANICALLY ACTIVATED COMPOSITIONS

Mechanical activation of combustible mixtures is their processing in high-speed planetary ball mills, vibrational mills, and other devices, where the particles of the mixture are subjected to mechanical impacts with a force sufficient for breakdown of brittle components and plastic deformation of viscous components [45]. Brittle components are milled to finer particles, whereas plastic components (usually, metals) are subjected to multiple flattening procedures, forming layered composites with the layer thickness decreasing as the activation duration is increased. Small fragments of brittle components are often found inside the particles of plastic reagents. Activation not only decreases the particle size of reagents, but also increases their contact area, the contact surface is cleaned from oxide films and other admixtures, defects of the crystalline structure are accumulated, and all these factors enhance the chemical activity of the combustible mixture [46, 47]. The stage of activation may include partial or complete dissolution of one reagent in the other (mechanical doping or mechanical fusion); otherwise, the components of the mixture can be involved into a chemical reaction with formation of a new compound (synthesis). In some cases, self-ignition of the mixture occurs directly in the course of activation. Thus, a natural question arises: which degree of fragmentation of the reactive heterogeneous composition can be reached before the reagents start to interact with each other? It will be further demonstrated that many papers provide direct evidence (electron microscope images, etc.) that mechanical activation can be used to obtain nanostructural reactive composites with the size of structural components (phases) of the order of 10–100 nm. Even in those cases where direct evidence was not given, however, mechanical activation led to significant changes in the properties of reactive mixtures, for instance, a decrease in the self-ignition temperature by hundreds of degrees. Let us note that the nanostructural state of the system is determined by drastic changes in its properties (melting point, reactivity, etc.) rather than by the "numerical" values of its characteristic size (1, 10, or 100 nm) [48, 49]. Based on this fact, let us consider the specific properties of the behavior of mechanically activated combustible compositions.

There are comparatively many publications on mechanical activation of combustible mixtures during the last decade. Comparisons of results obtained by different authors is difficult because the mechanical activation process depends on many parameters, including the velocity, acceleration, mass, size, and shape of the milling bodies, the geometric size of the facility, the mass ratio of the milling bodies (balls) to the activated mixture, the medium where the activation is performed (air, inert gas, vacuum, or liquid), and many others. Still, it is possible to identify three parameters that reflect the physical (not engineering) aspect of the process most obviously: the energy of one impact (collision between the balls or between the ball and the wall), frequency of collisions, and total time of activation. By multiplying these three parameters, we obtain the total energy spent on activation. IN reality, this does not mean that all energy is "pumped" into the activated mixture because the major part of this energy is converted to heat. Nevertheless, these three parameters and their product can be used as a physical basis for comparisons of results.

The reported results fall into two clearly distinguished groups in terms of the impact energy. The first group can be called low-energy activation, where the impact energy is 0.1–0.2 J, and the activation time ranges from minutes to tens of hours (note that the authors of these publications often speak about high-energy treatment, but we refer these processes to low-energy activation). The burning rates and temperatures for this group are shown in Fig. 8 as functions of time [50–54]. The second group of results is associated with high-energy activation, where the impact energy is 1–2 J, and the activation time ranges from several seconds to minutes; the combustion parameters of thus-activated compositions are presented in Fig. 9 [55–58].

As is seen from the figures, the burning rate of the absolute majority of the mixtures in the case of low-energy activation increases with increasing time of mechanical processing. The maximum burning rate also increases, but still remains lower than the adiabatic value for many of the compositions examined. For instance, the thermodynamic calculation of the adiabatic

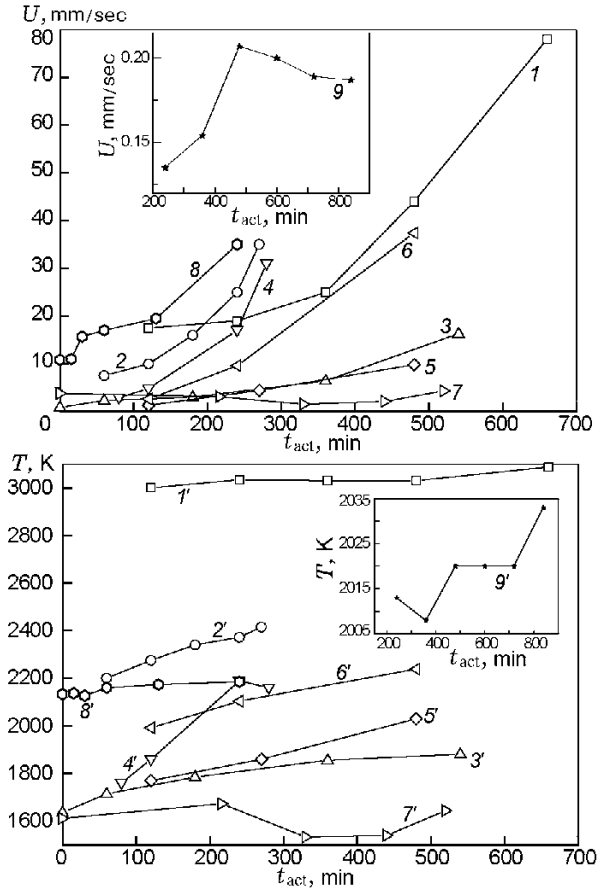

Fig. 8. Combustion parameters of mechanically activated compositions (low-energy activation): Ti + C [50] (1 and 1′); Ti + 0.43C [50] (2 and 2′); Nb + 2Si [51] (3 and 3′); 5Nb + 3Si [51] (4 and 4′); Ta + 2Si [52] (5 and 5′); 5Ta + 3Si [52] (6 and 6′); Ti + 2Si [53] (7 and 7′); 5Ti + 3Si [53] (8 and 8′); Si + C [54] (9 and 9′).

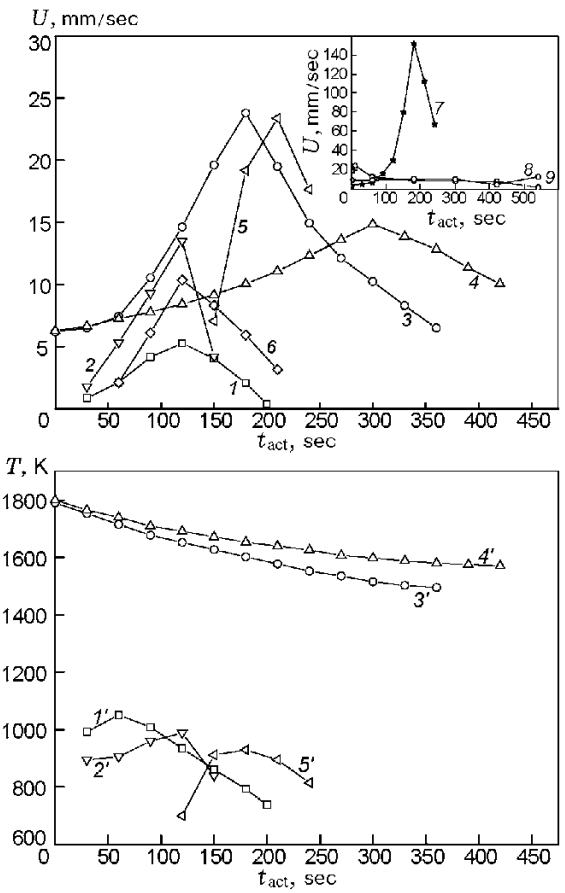

Fig. 9. Combustion parameters of mechanically activated compositions (high-energy activation): 3Ni + Al [55] (1 and 1′); 3Ni + Al [57] (2 and 2′); (Ti + 2.1B) + 60% Cu, acceleration of milling balls 60g [56] (3 and 3′); (Ti + 2.1B) + 60% Cu, acceleration of milling balls 40g [56] (4 and 4′); Ti + Ni [57] (5 and 5′); 4Ni + Si (Ni + 10% Si) (6); Ni + Al [57] (7); Ni + Al, activation in air [58] (8); Ni + Al, activation in argon [58] (9).

combustion temperature yields the value $T_{ad} = 3290$ K for the Ti + C composition, 1870 K for Nb + 2Si, 2290 K for 5Nb + 3Si, 1690 K for Ti + 2Si, and 2400 K for 5Ti + 3Si. It seems logically to assume that an increase in the reaction rate owing to mechanical activation for these compositions decreases the level of heat losses during combustion and increases the depth of conversion, which leads to an increase in the maximum temperature; thereby, the burning temperature approaches the adiabatic value, but does not reach the latter. For other systems, the burning temperature could be higher than the adiabatic temperature. These systems include Ta + 2Si ($T_{ad} = 1794$ K), 5Ta + 3Si ($T_{ad} = 1823$ K), and Si + C ($T_{ad} = 1873$ K). It is possible to argue that the excess of the burning temperature over the adiabatic value is an indication of the excess energy accumulated by crystal lattices of reagents during mechanical processing?

In our opinion, this conclusion is premature. There are at least three sources of errors: (1) error of thermodynamic calculations owing to inaccuracies of thermodynamic functions for the chosen substances at high temperatures; (2) inaccuracy of temperature measurements, especially with the use of pyrometry [52]; (3) uncertainty of the initial temperature. The latter error could appear, in our opinion, because cylindrical samples 8 mm in diameter and 10 mm long were ignited by a heated spiral located at a distance of 1 mm from the end face of the cylinder [52]. As there was no direct contact between the spiral and the sample, the sample could be heated comparatively slowly, and the heat penetrated into the sample to a considerable depth, thus, increasing its initial temperature. Therefore, additional

investigations are necessary to make a grounded conclusion about the influence of energy stored in solid components in the course of mechanical activation on the burning temperature.

The dependences obtained after high-energy activation are qualitatively different (see Fig. 9). The burning rates have maximums at activation times of 120 to 300 sec. The decrease in the burning rate at long times of mechanical activation is usually explained by the formation of the reaction products already at the stage of activation. The temperature curves for some systems also have maximums; as is seen from the figure, the maximum of the temperature curve can differ from the maximum of the burning rate for the same composition. A monotonic decrease in the burning temperature was observed for Ti–B–Cu compositions. In all cases, the maximum burning temperature measured by thermocouples was lower than the adiabatic value. It should be noted that an increase in the burning rate is observed at the limit of combustion for compositions providing weak burning without activation because of the low thermal effect (curves 1–6) or low density (curve 7). In those cases where the initial mixture corresponded to stoichiometry with the maximum heat release and was pressed to the optimal density (curves 8 and 9), the increase in the burning rate was not observed [58]. Mechanical activation of weakly exothermal compositions makes it possible to increase the level of conversion and to decrease the contents of secondary phases [59].

It was noted in many papers that mechanical activation leads to a drastic decrease in the self-ignition temperature usually determined by the DTA method. For instance, the self-ignition temperature for the Ti–C system decreased from 1600 K for non-activated mixtures to 770 K after low-energy activation during 5–10 h [50]; the corresponding decrease for the Ti–Si system was from 1670 to 870 K after several hours of activation [60]. For the Ti–Si–C system (with the composition 3Ti + Si + 2C), the self-ignition temperature decreased from 1190 to 430 K (90 min of activation), and spontaneous ignition of the mixture occurred directly in the milling drum at a temperature of 340 K at the 106th minute of activation [61].

Investigations are performed to combine mechanical activation with other types of activating effect, which allows the domain of combustion to be further expanded. One of the research directions is chemical activation. Addition of several percent of NH_4Cl to the mechanically activated mixture Si + C allowed initiation of combustion at room temperature (this composition usually requires significant heating) and obtaining fine-grain silicon carbide [62, 63]. By adding KNO_3 (20 wt.%) to the Fe–Si system, stable combustion was provided and iron silicides with a fine-grain microstructure were obtained [64]. Combustion of the 4B + C [65], Fe + Al [66], and 2Mg + Ni [67] compositions was additionally activated by passing electric current through the sample subjected to preliminary mechanical activation. The activating effect of electric current is not restricted to the Joule heating of the entire sample; most probably, constant or pulsed current generates spark and arc microdischarges at places of contact of the reactive mixture particles. This phenomenon formed the basis of the method of plasma-spark activation combined with mechanical activation, which was used, in particular, to obtain the TiC–TiB_2 cermet [68] and dense nanocrystalline $MoSi_2$ [69] in the burning regime. In some publications, these methods of activation are additionally combined with a mechanical action on condensed combustion products of hot pressing [66–68] or extrusion [70].

Mechanical activation of thermite-type compositions is a separate aspect of activities in this field. Aluminothermic systems were reviewed in [71]. Thermite systems usually burn vigorously, with considerable heat release, and do not require additional activation for obtaining a self-sustained reaction. Mechanical activation is used for these systems to obtain either fine-grain (nanocrystalline) products, for instance, the Al_3Ni/Al_2O_3 nanocomposite [72], or a superactive thermite composition. The latter circumstance is closely related to the above-considered nanothermites (superthermites), where mechanical activation is used as a method for obtaining nanothermites [72–76]. For this purpose, the critical time necessary for self-ignition of the Me_1 + Me_2O_x system during mechanical mixing is determined first (usually, tens of minutes). After that, mechanical activation is "arrested" (arrested reactive milling) approximately in the middle of this period to obtain a certain half-finished product in the form of micron-sized composite particles with a small (beginning from several nanometers) size of crystallites, depending on mechanical activation conditions. An increase in the burning rate for mechanically activated compositions was reported, and fairly moderate burning rates (≈0.5 m/sec for Al—Fe_2O_3 [74]) were given. The activation energies of ignition were determined: ≈150 kJ/mole for the Al–MoO_3 nanothermite and 170 kJ/mole for Al–Fe_2O_3. These values are close to the activation energies of ignition for non-activated thermites, for instance, ≈170 kJ/mole for the Al–Fe_2O_3 system [77].

Another group of mechanically activated combustible compositions is composed of hybrid systems (solid fuel–gaseous oxidizer–solid product) reacting in the filtration combustion mode. Mechanical activation

of a mixture of Si and α-Si_3N_4 with addition of 4–5% NH_4Cl during several hours made it possible to obtain combustion of this mixture in nitrogen at a pressure of 1–3 MPa, which is substantially lower than the pressure necessary for combustion of non-activated silicon in nitrogen [78, 79]. A similar approach was developed for synthesis of β-sialons ($Si_6Al_zO_zN_{8-z}$, $0 < z \leqslant 4.2$). In that case, a mixture of silicon, aluminum, and aluminum oxide was subjected to activation in a planetary ball mill, and combustion took place in a nitrogen medium at a pressure of 1 MPa [80, 81]. Mechanical activation of the mixtures of Y_2O_3, Si, Al, SiO_2, α-Si_3N_4, and stearic acid ($CH_3(CH_2)_{16}COOH$) made it possible [82] to obtain a composition burning in air at a standard pressure and forming α-sialon. Another approach includes mechanical activation of the metal fuel (e.g., titanium powder) in a gaseous oxidizer (nitrogen) medium until self-ignition occurs. Nano-sized TiN [83] and cermets on the basis of TiC_xN_{1-x} [84] were obtained by this method. The laws of combustion of hybrid systems on the basis of mechanically activated powders and, moreover, combustion directly during mechanical activation have been little studied yet.

Summarizing this paragraph, we can state that mechanical activation (i) decreases the temperature of self-ignition of various combustible systems, (ii) expands the flammability limits, (iii) favors a more complete reaction, and (iv) sometimes increases the combustion wave front velocity. What is the mechanism of these effects? There are several explanations in publications.

The first explanation is obtaining of reactive media with nanoscale heterogeneity, which enhances the reactivity of these mixtures. Most authors determine the crystallite sizes in activated mixtures on the basis of broadening of X-ray diffraction peaks with the use of the Sherrer formula [85] or by the Williamson–Hall method [86]. These methods provide indirect evidence, because broadening of the peaks can be caused not only by small sizes of crystallites and stresses in the crystal lattice, but also by inhomogeneity of sizes or chemical composition (within the range of homogeneity). A direct method is transmission electron microscopy, but this it an expensive and labor-consuming method, and only few authors give TEM results for mechanically activated mixtures [58, 69], which confirm the presence of particles or crystallites of the order of 100 nm or smaller. Thus, we have to admit that the assumption about the nanostructural components in reactive mixtures after their mechanical activation is based in most cases on indirect data: broadening of X-ray diffraction peaks and drastic changes in properties (ignition temperature) of these compositions. Further investigations are necessary to draw more definite conclusions.

The second explanation involves the formation of unstable solid solutions. Wen et al. [87] studied the mixture of Al : Ti 3 : 1 and stearic acid ($CH_3(CH_2)_{16}COOH$), which was used as a controlling agent preventing cold welding of metal particles. This mixture was subjected to mechanical activation in an argon medium. After 100 h of mechanical activation, the X-ray diffraction analysis revealed the emergence of a new phase, which could be identified in terms of its lattice parameters as an oversaturated solid solution of titanium in the FCC lattice of aluminum. The size of crystallites of this phase, which was determined by the Sherrer formula [85], was extremely small (3.8 nm). Moreover, such solutions cannot exist in accordance with the equilibrium diagram of state. A TEM analysis of particles confirmed the formation of such a nonequilibrium solution with nano-sized crystallites. It is important that these particles turned out to be highly reactive: the action of an electron beam with a current density of $\approx$20 pA/cm^2 during 1 sec was sufficient for "self-ignition" of the solution, with formation of the equilibrium Al_3Ti phase with the particle size of several nanometers. Thus, it was demonstrated that mechanical activation can lead to formation of nonequilibrium oversaturated solutions with small-sized crystallites, which can possess unique reactive properties owing to structural changes. Based on these results, the parameters of ignition and combustion of such nonequilibrium oversaturated nanocryctallite solutions in various oxidizer media (air, oxygen) were further investigated [88–91]. For instance, Shochin et al. [88] prepared a nonequilibrium solution in the Mg—Al (10–50% Mg) by this method. The ignition temperatures of these solutions ($\approx$1000 K) turned out to be substantially lower than that for aluminum ($\approx$2300 K). Qualitatively similar results were also obtained in Al–Ti, Al–Li, and Al–Zr systems [89–91].

Many authors also indicate that mechanical deformation ensures a clean contact surface of the reagents, free from oxides and contamination, which enhances the reactivity of the mixtures. This hypothesis also requires experimental validation and quantification.

As is seen from the discussion above, the assumption about the key role of "pumping" of additional energy, which is stored in defects of crystalline structures of the mixture components, has not yet found reliable experimental validation (in the form of an increase in temperature above the adiabatic value or other effects).

The nature of "ageing" of activated compositions (gradual reduction of their activity with time after activation) is not elucidated either. This effect can be attributed to relaxation of defects of the crystalline structure, decomposition of unstable solid solutions, passi-

vation (e.g., oxidation) of clean contact surfaces, and other processes.

The mathematical model of combustion of activated mixtures [92] is based on taking into account three basic effects: pumping of excess energy into the mixture, increase in the contact surface area (fragmentation of the reagents), and changes in the activation energy of the chemical reaction. This model was later extended by including the heat of phase transitions [93]. As a whole, this model yields reasonable and predictable results: an increase in the burning rate with increasing surface area of the reagents, with increasing excess energy of the mixture, etc. Some features of propagation of gasless combustion waves in mechanically activated (structured) systems, especially at the microscopic level, are successfully explained by the microheterogeneous (discrete) model [94]. The discrepancy between the experimental results and theoretical models of the process is still too large to allow precise quantitative modeling of the process.

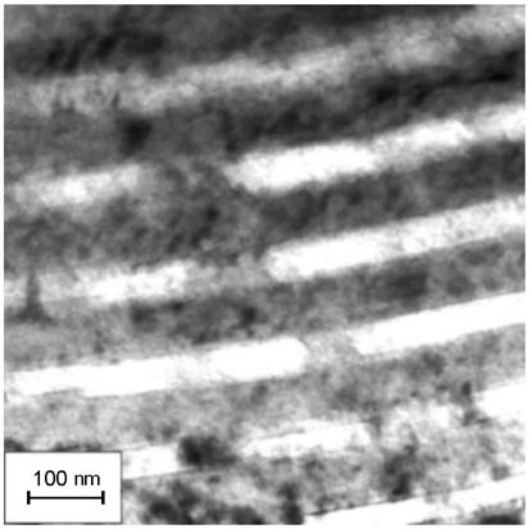

Fig. 10. Microstructure of reactive multilayer nanofilms of the Ti/Al system [95, 99].

COMBUSTION OF MULTILAYER NANOFILMS

A new class of combustible systems is composed of reactive multilayer nanofilms consisting of alternating nano-sized layers of reagents capable of exothermal reactions in the combustion mode. The basic method of obtaining such films is layer-by-layer magnetron-assisted deposition. Two magnetron sources operate simultaneously in the deposition chamber: one spraying the reagent A, and the other spraying the reagent B; the flows of the sprayed atoms are separated in space and do not mix with each other. The substrate used for deposition is mounted on a rotating table so that it is alternatively located in the flow of the atoms A (deposition of the layer of the solid reagent A) and then in the flow of the atoms B (deposition of the layer of the reagent B above the previously deposited layers). This method allows obtaining continuous layers with a thickness of 3–4 nm and more, and the number of layers reaches several thousands. An example of the microstructure of a reactive multilayer nanofilm is shown in Fig. 10. A detailed review of methods of obtaining such films, reaction mechanisms, and formation of the structure of the products can be found in [95]. In this paper, we consider some aspects associated with the laws of combustion of such multilayer systems.

The process of combustion in multilayer nanofilms was first realized and patented by American researchers in 1996 [96]. They found that a reaction wave can be initiated by means of short-time local heating of multilayer nanofilms by an electric spark, a laser pulse, or a glower; after initiation, this reaction wave propagates over the entire film and does not need external sources of heat. The self-sustained character of the process, the presence of the wave front clearly seen as luminescence of solid incandescent reaction products, a drastic increase in temperature in the front by 1000–1500 K, and almost instantaneous formation of solid combustion products behind the wave front allow this phenomenon to be classified as gasless combustion [97]. Figure 11 shows the video frames of the process and the quenched front of the combustion wave in multilayer nanofilms.

The parameters of propagation of the combustion wave front, which are typical for reactive multilayer nanofilms, differ from those of systems with a similar composition obtained by mixing of powders. Available data [98–104] on the burning rate, temperature, and regimes are summarized in Table 2. The burning rates usually observed are higher and the maximum temperatures are lower than the corresponding values for powder systems. As is seen from Table 2, only few systems have been studied so far. One of the main reasons for that is the technological difficulties of production of reactive multilayer structures. It is sufficient to stir powder reagents to obtain the initial reactive compositions, whereas fabrication of multilayer nanofilms requires careful selection of spraying regimes for each reagent, as well as appropriate magnetron targets and substrates. In addition, not all pairs of reagents are suitable for obtaining multilayer films with a desired structure and mechanical properties. Crystallographic discrepancy of the structure, differences in the thermal

TABLE 2

Parameters of Combustion of Multilayer Nanofilms

System	Burning rate, m/sec	Burning temperature, K	Combustion mode	Reference
Ni–Al	0.6–10	—	Stationary	[98]
Ti–Al	0.05–0.5	1360	Stationary, pulsed, spin (?)	[99]
Pt–Al	40–80	—	Stationary	[100]
Co–Al	0.5–9	—	—//—	[101]
Ni–Si	20–30	1 565	—//—	[102]
Nb–Si	0.3–4	—	—//—	[103]
3CuO + 2Al	1	—	—	[104]

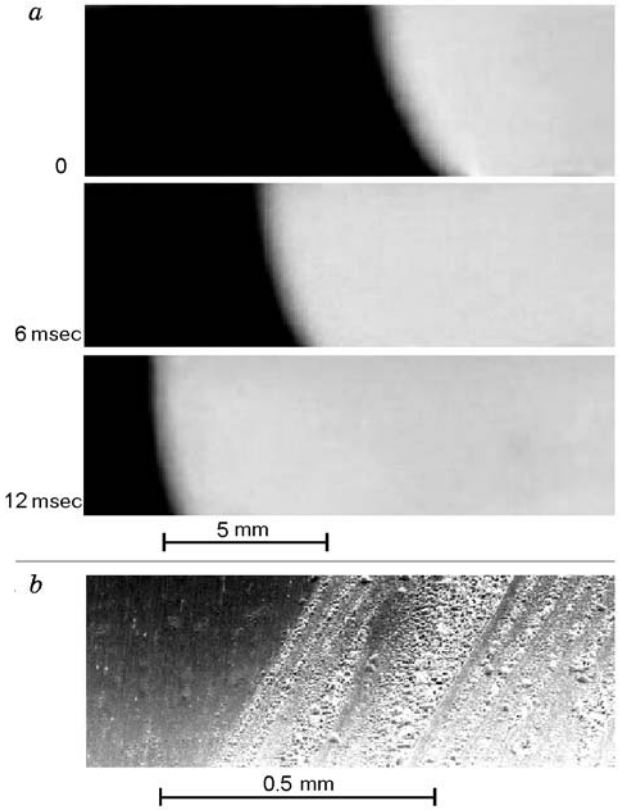

Fig. 11. Video frames of the combustion wave in reactive multilayer Ti/Al nanofilms (a) and quenched wave in this system (b) [95, 134].

expansion coefficients and mechanical properties, and other factors can break the layers or the entire film already at the stage of film production (deposition) or during an attempt of combustion initiation. For instance, multilayer films of the Ti–C system with a total thickness of ≈1 μm are obtained by means of magnetron deposition, but local heating makes the film immediately tear off and roll into a "tube." For this reason, combustion wave propagation to macroscopic distances (at least, several millimeters) could not be obtained. For another popular system, Ti–B, it is impossible to obtain a multilayer film because of the problems of magnetron spraying and deposition of boron. Nevertheless, the number of gasless systems used to prepare multilayer nanofilms permanently increases, and the research in this field is pursued.

Because of intense luminescence of the reaction wave front, it is comparatively easy to measure the burning rates of reactive multilayer nanofilms, which is usually performed by methods of high-speed video filming or on the basis of signals from a photodetector array. The temperature measurement is a more complicated problem. Even thermocouples with thin junctions welded to foil give underestimated values of temperature because of heat removal and interfere with the combustion process. Pyrometric methods require special calibrations to take into account the emissivity of the film material. For this reason, the data on temperature in Table 2, which were obtained by optical pyrometry methods, are not very exact.

The dependences of the burning rate on the layer thickness reported in many publications are summarized in Fig. 12. It is seen that almost all dependences have maximums in the range of 10–50 nm, which, in our opinion, can be attributed to the presence of a thin layer (about 0.1–1 nm, independent of the thickness of individual layers) between the surfaces of the reagents, where the atoms have partly reacted already at the deposition stage. This reacted layer acts both as a diffusion barrier preventing interaction of reagents in the combustion wave front and as an inert diluent, and the relative fraction of this layer increases as the thickness of the main layers is reduced. Therefore, both the burn-

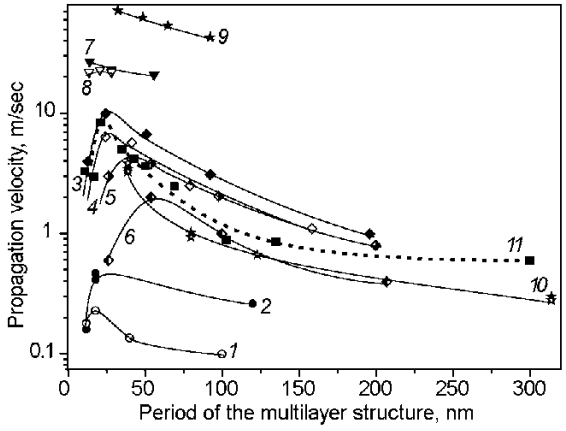

Fig. 12. Velocity of reaction wave propagation versus the period of the multilayer structure (total thickness of two adjacent layers): Ti/Al film, $T_0 = 473$ K, spark ignition [99] (1); Ta/Al film, $T_0 = 473$ K, ignition by a heated tungsten wire [99] (2); Ni/Al film after deposition, $T_0 = 298$ K [98] (3); Ni/Al film after annealing at 423 K during 90 min [98] (4); Ni/Al/ film after annealing at 423 K during 6 h [98] (5); Ni/Al film after annealing at 423 K during 24 h [98] (6); 2Ni/Si film with a total thickness of 1.62 μm, $T_0 = 298$ K, laser ignition [102] (7); 2Ni/Si film with a total thickness of 0.73 μm, $T_0 = 298$ K, laser ignition [102] (8); Pt/Al film, $T_0 = 298$ K, laser ignition [100] (9); Nb/Si film, $T_0 = 298$ K [103] (10); Co/Al film with a total thickness of 7.5 μm [101] (11).

ing temperature and burning rate are seen to decrease if the layer thickness is extremely small. The fact that it is the reacted layer that decelerates the combustion process is also evidenced by the decrease in the burning rate of annealed samples (curves 3–6 in Fig. 12), because annealing increases the reacted layer thickness. Obviously, the decrease in the burning rate on the right of the maximum, i.e., with increasing layer thickness, is associated with an increase in the characteristic diffusion scale of the reactive system, which leads to a decrease in the effective rate (macrokinetics) of heterogeneous interaction [105].

Among Al-containing systems used to obtain multilayer nanofilms, the Ni–Al system has the greatest reaction heat, and the combustion wave propagation velocities measured in this system are substantially higher than the values obtained in powder systems with the same composition. Thus, the reaction front velocity was ≈4 m/sec, with the total thickness of the film being within 300 nm [106]. It was also shown that the dependence of the reaction wave propagation velocity on the thickness of the layers in metal–aluminum systems reached the maximum value if the total thickness of two layers of the reagents (A + B) is 25–30 nm. A decrease in the burning rate with increasing thickness of the layers for Ni/Al and 3Ni/Al compositions was noted in [107].

The question of the limit of existence of self-sustained reactions with increasing thickness of the nickel and aluminum layers in layered systems has not yet gained any definite answer. As it is difficult to obtain comparatively thick (above 1 μm) layers by means of spraying, the studies are performed with piled or stranded foils. Combustion of thus-obtained layered systems with a thickness of metal foils of ≈50 μm was studied in [105, 108]. It was shown that the system had to be heated to a temperature of 540 °C to ensure stationary propagation of the reaction front under the examined conditions. The burning rates observed were ≈0.5 cm/sec. The model proposed in [105, 108] allows the burning rate in layered systems to be estimated as a function of the thickness of the reagent layers. The model is based on the kinetic data obtained in [109, 110], which indicate that the leading stage of interaction in binary systems with melting of one component in the heating zone is the dissolution of the high-melting-point component in this melt. In the case considered, this stage is the dissolution of nickel in the aluminum melt (first-order reaction with an almost zero activation energy). Based on these assumptions, Shteinberg et al. [105] proposed a simple formula for determining the burning rate in such systems

$$U_\mathrm{b} = (aD_L)^{0.5}/\delta, \qquad (1)$$

where a is the thermal diffusivity of the reactive medium, δ is the thickness of the aluminum layer, and D_L is the diffusion coefficient in the fluid. As was shown [109], in a wide range of variation of the individual layer thicknesses (from 50 μm) to 50 nm) and burning rates (from 0.5 to 5 m/sec), the experimental points on gasless combustion in the Ni–Al system reported in different papers, including [106, 107] mentioned above, are well approximated by a straight line in the coordinates $U_\mathrm{b} = F(1/\delta)$; the calculation based on the slope of this straight line by Eq. (1) yields $D_L \approx 10^{-5}$ cm^2/sec.

These activities recently gained more applications owing to the development of rolling methods. Qiu and Wang [111] obtained a multilayer Ni/Al film by the method of multiple cold rolling; the total thickness of the film was about 200 μm, and the layer thickness was approximately 1–10 μm, as it follows from the microstructures presented in that paper. When the film was heated in the flame, comparatively slow propagation of the first "reaction front" was observed during several seconds, and the film surface became dark. Then, the second reaction front having a red color prop-

agated "very rapidly" over the entire film. No quantitative data were given in [111] for these reaction waves.

The Ti–Al system ensures a lower heat release than the Ni–Al system. For instance, the adiabatic burning temperature is 1912 K for the Ni–Al composition and only 1519 K for the Ti–Al system. The curve of the burning rate as a function of the layer thickness [99] has a similar shape to that of the Ni–Al system, with a maximum around 20 nm. It is interesting that the burning rate depends on the method of reaction initiation.Identical samples initiated by a spark and by a hot wire have different burning rates. This may indicate nonuniqueness of reaction wave propagation regimes. It was noted that samples initiated by a wire practically do not change their appearance during combustion, and their surface remains smooth. Samples initiated by a spark slightly warp, and their surface becomes rough after combustion. At the same time, the X-ray diffraction analysis showed that the phase composition of the products is identical for all methods of initiation.

Rogachev et al. [99] also determined the burning rates (in vacuum) as functions of the initial temperature for reactive multilayer Ti/Al nanofilms. Stationary combustion was observed in the range of initial temperatures from 400 to 600 K. Below 400 K, stationary propagation of the wave could not be realized in these films, and self-ignition of the films occurred when the initial temperature of ≈600 K was reached. Thus, the temperature of self-ignition in such layered nanosystems is 300–400 K lower than the value at which self-ignition (thermal explosion) occurs in powder mixtures with micron-sized particles of reagents [112].

Extremely high burning rates were registered in films of the Pt–Al system. The burning rates above 70 m/sec [100] were later confirmed in [113] where record-beating velocities of the gasless combustion wave in Pt/Al films were obtained: from 20 to 90 (!) m/sec, depending on the thickness of the layers and the total thickness of the film. The films were ignited by a short pulse of laser radiation on a (Si—SiO_2) substrate without additional heating. These results require experimental validation and also explanations of the anomalously high reaction rates obtained.

The laws of combustion of the Co–Al system [101] are similar to those in the Ni–Al system. The temperature of self-ignition of multilayer Co/Al films was measured as a function of the layer thickness. The self-ignition temperature was demonstrated to decrease monotonically from 720 K for the total thickness of two layers (Co + Al) of 250–300 nm to 510 K for the total thickness of the layers equal to 5 nm.

The data on propagation of reaction waves in the Ni–Si system were obtained with the use of high-speed video filming [103] (curves 7 and 8 in Fig. 12) with a frequency of 6000 frames per second. Based on the video frames reported in [103], the width of the luminescent zone was approximately 3–4 mm, and the propagation velocity was 23 m/sec; therefore, the characteristic reaction time can be estimated as 0.1 msec. High-speed pyrometric measurements showed that the time of existence of the high-temperature zone is much shorter.

The burning rate of multilayer Nb–Si films was measured by an array of optical fibers arranged in a row along the reaction wave direction; the fiber outputs were connected to a photodiode [103]. The transition of the luminescent front near each fiber induced a jump of the electric signal from the photodiode, which was registered by an oscillograph. It is seen from Fig. 12 (curve 10) that the burning rate in this system is lower than in the Ni–Si system, though the adiabatic temperature of combustion of the Nb–Si system is higher than that of the Ni–Si system.

Multilayer nanofilms were also obtained in the Ti–Si system, but the data on characteristics of the self-propagating process are rather approximate: the reaction propagated to a 1-cm distance within a fraction of a second [114]. A similar situation is also observed for several more systems, for instance, for Ni–Ti. Powder mixtures of Ni and Ti are well known in the theory and practice of self-propagating high-temperature synthesis [115]; they are used for synthesis of titanium nickelide, which is an intermetallic compound with the shape memory effect. Obtaining of the same compound from thin multilayer films (up to 100 alternating layers of Ni and Ti) was proposed as a new method in [116], but the process of combustion wave propagation in these films was not studied.

The thermite-type CuO_x–Al system is characterized by intense heat release during the reaction (e.g., the adiabatic temperature of combustion of the 3CuO + 2Al composition is 2840 K). Multilayer films obtained in this system by the method of magnetron spraying [104] had a total thickness of the layers CuO_x + Al of the order of 1000 nm. The velocity of reaction wave propagation without additional heating in such films was 1 m/sec.

We should also mention the papers on combustion of comparatively thin (of the order of 100 μm) layers of the Ti–B powder mixture [117] and porous Ti + 2B films 230 μm thick, which were obtained by the method of rolling from the corresponding powders [118, 119]. The burning rates of these objects turned out to be commensurable with the burning rates of the usual powder samples with the same composition (≈0.1 m/sec), and the microstructures of the initial films and the products are closer to the traditional powder compositions than

to multilayer films considered in the present review.

There are many publications dealing with the mechanism of combustion of reactive multilayer nanofilms, in particular, mathematical modeling of this process. Most of them are based on the well-known layered model of combustion [120, 121], where the reactive medium is presented in the form of alternating layers of the fuel and oxidizer, aligned parallel to the direction of combustion wave propagation.The solid product is formed on the interfaces between the layers of the reagents, and the diffusion-controlled reaction occurs owing to diffusion of the reagents through the layer of the product in the direction perpendicular to the interface between the layers. At first glance, the layered model is perfectly suitable to describe reactive multilayer films. In contrast to heterogeneous combustible compositions and an irregular microstructure (gunpowders, powder mixtures), where the layered model is used to obtain an approximate description of the microstructure, the layered model in the case of multilayer films coincides with the real microstructure of the reactive medium. Nevertheless, it is necessary to consider whether it is admissible to use the macrokinetic layered model for systems with nano-sized layers. An analysis of the layered model of combustion for a heterogeneous reaction [122–124] controlled by the reactive diffusion mechanism showed that the wave propagation velocity is inversely proportional to the total thickness of two adjacent layers of the reagents (d). The burning rate is described by the equation

$$U = \frac{4\lambda T_c}{d}\left(\frac{3k_0R}{E(T_c - T_0)}\right)^{1/2}\exp\left(-\frac{E}{2RT_c}\right), \qquad (2)$$

where λ is the thermal conductivity of the medium, T_c and T_0 are the combustion temperature and the initial temperature, respectively, k_0 is the pre-exponent in the Arrhenius law, E is the activation energy, and R is the gas constant. To adapt the layered model to very thin (nano-sized) layers, the model was supplemented with the previously mentioned partly reacted layer along the interface between the reagents. The presence of this layer in the initial reactive multilayer nanofilms was validated by TEM and DSC experiments [125, 126]. If the thickness of this layer is small, as compared with the layered structure period, the wave propagation velocity follows Eq. (2) with E and k_0 being understood as the activation energy and pre-exponent for volume diffusion. When the period of the structure becomes smaller than 10–20 nm, the influence of the mixed layers leads to a drastic decrease in the wave velocity.

The calculations performed within the framework of the layered model [98, 125] provided reasonable agreement with experimental data for the Ni–Al system. It should be noted, however, that the layered model [125] contains a number of parameters that can be defined arbitrarily or in comparatively wide ranges, for instance, the initial thickness of the reacted layer and the profiles of concentrations inside this layer (linear, exponential, etc.), diffusion activation energy, and pre-exponent.

There are some recent theoretical publications where many specific features of combustion of reactive multilayer nanofilms were reproduced by methods of computer modeling. Jayaraman et al. [127] showed that an increase in the mass fraction of the inert product in the initial sample leads to the loss of stability and to the transition of combustion to a self-oscillatory mode. An increase in the ambient temperature (i.e., reduction of heat losses) decreases the amplitude of oscillations and stabilizes the combustion. The roughness of the reactive layers and the inhomogeneity of their composition enhance the amplitude of oscillations.These results agree with experimental observations of the oscillatory combustion mode in Ti/Al nanofilms [99] and also the traces of self-induced oscillations in combustion products of Zr/Al/(CuNi) [128] and Ti/Al [129] films.

The effect of radiative and conductive heat losses on the burning rate of multilayer nanofoils was studied theoretically [130]. The model predicts that more intense heat losses leads to a decrease in the burning rate and the amplitude of velocity oscillations, while the period of oscillations increases. Jayaraman et al. [130] took into account the effect of melting of a thin additional layer (Ni, Cu, or Sn) on the foil surface, which can either quench or enhance the oscillations. According to this model, melting of one of the reagents or synthesis products reduces the mean burning rate [131]. Makino [132] performed mathematical modeling of combustion of a three-species reactive multilayer nanofilm consisting of alternating layers of the pure reagent and layers of a two-species alloy.

Thus, it may seem that theoretical papers published during the last decade adequately describe all known regimes of gasless combustion of multilayer nanofilms. A detailed analysis, however, shows that this is not so. First of all, to obtain the calculated burning rates that coincide with experimental measurements, the authors of the theoretical papers [127–132] have to use strongly overestimated values of the diffusion coefficients (sometimes, by several orders of magnitude). The validity of these assumptions is no obvious. The arguments about faster diffusion of atoms in nano-sized systems owing to a greater concentration of defects ar not supported by quantitative data for partic-

ular phases in the systems considered. Many of the examined systems contain aluminum (see Table 2) whose melting point is much lower than the burning temperature. Therefore, the mechanism of dissolution of the high-melting-point reagent in the melt and crystallization of the solid product inside the melted layer can turn out to be the basic mechanism in combustion of these reactive multilayer nanofilms, whereas this mechanism is ignored in the proposed layered models, except for that in [105]. Finally, the formation of a continuous layer of solid products along the reagent boundaries has not yet found direct experimental confirmations. Electron microscope investigations of intermediate (quenched) and final products of combustion reveal the formation of individual islands, grains, or columnal structures aligned perpendicular to the layers [133, 134, 101], which obviously contradicts the proposed layered models. Apparently, further experimental studies of combustion and structure formation in reactive multilayer nanofilms can be expected to reveal new specific features of the mechanisms of nanoheterogeneous reactions, which will assist in developing more adequate theoretical models.

The authors express their sincere gratitude to Prof. A. S. Shteinberg for the interest in this work and useful discussions.

This work was supported by the Russian Foundation for Basic Research (Project Nos. 08-03-00890 and 10-03-00217).

REFERENCES

1. L. E. Fried, M. Riad Manaa, P. F. Pagoria, and R. L. Simpson, "Design and synthesis of energetic materials," *Annu. Rev. Mater. Res.*, **31**, 291–321 (2001).
2. A. A. Gromov, T. A. Khabas, A. P. Il'in, et al., *Combustion of Metal Nanopowders* [in Russian], Deltaplan, Tomsk (2008).
3. W. Fahrner (ed.) *Nanotechnology and Nanoelectronics*, Springer-Verlag, Berlin; New York (2005).
4. C. Dubois, P. G. Lafleur, and C. Roy, "Polymer grafted metal nanoparticles for fuel applications," *J. Propulsion Power*, **23**, No. 4, 651–658 (2007).
5. J. J. Granier and M. L. Pantoya, "Laser ignition of nanocomposite thermites," *Combust. Flame*, **138**, 373–383 (2004).
6. M. L. Pantoya and J. J. Granier, "Combustion behavior of highly energetic thermites: nano versus micron composites," *Propellants, Explosion, Pyrotechnics*, **30**, No. 1, 53–62 (2005).
7. M. L. Pantoya and J. J. Granier, "The effect of slow heating rates on the reaction mechanism of nano and micro composite thermite reactions," *J. Therm. Anal. and Calorimetry*, **85**, No. 1, 37–43 (2006).
8. B. S. Bockmom, M. L. Pantoya, S. F. Son, et al., "Combustion velocities and propagation mechanisms of methastable interstitial composites," *J. Appl. Phys.*, **98**, 1–7 (2005) — 064903.
9. B. W. Asay, S. F. Son, J. R. Busse, and D. M. Oschwald, "Ignition characteristics of metastable intermolecular composites," *Propellants, Explosives, Pyrotechnics*, **29**, No. 4, 216–219 (2004).
10. K. C. Walter, D. R. Pesiri, and D. E. Wilson, "Manufacturing and performance of nanometric Al/MoO_3 energetic materials," *J. Propulsion Power*, **23**, No. 4, 645–650 (2007).
11. S. F. Son, B. W. Asay, T. J. Foley, et al., "Combustion of nanoscale Al/MoO_3 thermite in microchannels," *ibid.*, pp. 715–721.
12. V. E. Sanders, B. W. Asay, T. J. Foley, et al., "Reaction propagation in four nanoscale energetic composites (Al/MoO_3, Al/WO_3, Al/CuO, and Bi_2O_3)," *ibid.*, pp. 707–714.
13. J. A. Puszinski, C. J. Bulian, and J. J. Swiatkiewicz, "Processing and ignition characteristics of aluminum-bismuth trioxide nanothermic system," *ibid.*, pp. 698–706.
14. K. B. Plantier, M. L. Pantoya, and A. E. Gash, "Combustion wave speeds of nanocomposite Al/Fe_2O_3: the effect of Fe_2O_3 particle synthesis technique," *Combust. Flame*, **140**, 299–309 (2005).
15. B. Mehendale, R. Shende, S. Subramanian, et al., "Nanoenergetic composite of mesoporous iron oxide and aluminum nanoparticles," *J. Energ. Mater.*, **24**, 341–360 (2006).
16. A. Prakash, A. V. McCormick, and M. R. Zachariah, "Aero-sol-gel synthesis of nanoporous iron-oxide particles: a potential oxidizer for nanoenergetic materials," *Chem. Mater.*, **16**, 1466–1471 (2004).
17. W. L. Perry, B. L. Smith, C. J. Bulian, et al., "Nanoscale tungsten oxides for methastable intermolecular composites," *Propellants, Explosives, Pyrotechnics*, **29**, No. 2, 99–105 (2004).
18. J. J. Kingsley and K. C. Patil, "A novel combustion process for the synthesis of fine particle α-alumina and related oxide materials," *Mater. Lett.*, **6**, 427–432 (1988).
19. K. C. Patil, M. S. Hegde, Rattan Tanu, and S. T. Aruna, *Chemistry of Nanocrystalline Oxide Materials: Combustion Synthesis, Properties and Applications*, World Scientific Publ. Co, Inc, Singapore (2008).
20. S. T. Aruna and A. S. Mukasyan, "Combustion synthesis and nanomaterials," *Curr. Opinion in Solid State and Mater. Sci.*, **12**, 44–50 (2008).
21. R. M. Cornell, *The Iron Oxides*, Wiley-VCH, Weinheim (2003).
22. E. L. Dreizin, "Phase changes in metal combustion," *Prog. Energy and Combust. Sci.*, **26**, No. 1, 57–78 (2000).

23. A. Varma, A. S. Mukasyan, K. Deshpande, et al., "Combustion synthesis of nanoscale oxide powders: mechanism, characterization and properties," *Mater. Res. Soc. Symp. Proc.*, **800**, 113–124 (2007).
24. A. S. Mukasyan, P. Epstein, and P. Dinka, "Solution combustion synthesis of nanomaterials," *Proc. Combust. Inst.*, **31**, No. 2, 1789–1795 (2007).
25. A. S. Mukasyan and P. Dinka, "Novel approaches for solution combustion synthesis of nano-materials," *Intern. J. Self-Propagating High-Temperature Synthesis*, **16**, No. 1, 23–35 (2007).
26. K. C. Patil, S. T. Aruna, and S. Ekambaram, "Combustion synthesis," *Curr. Opinion in Solid State and Mater. Sci.*, **2**, 158–165 (1997).
27. K. C. Patil, S. T. Aruna, and T. Mimani, "Combustion synthesis: an update," *Curr. Opinion in Solid State and Mater. Sci.*, **6**, 507–512 (2002).
28. K. Deshpande, A. S. Mukasyan, and A. Varma, "Direct synthesis of iron oxide nanopowders by combustion approach: reaction mechanism and properties," *Chem. Mater.*, **16**, No. 24, 4896–4904 (2004).
29. K. Wieczorek-Ciurowa and A. J. J. Kozak, "The thermal decomposition of $Fe(NO_3)_{(3)}9H_{(2)}O$," *Thermal Anal. Calor.*, **58**, 647 (1999).
30. A. G. Gasparyan and A. S. Shteinberg, "Macrokinetics of reaction and thermal explosion in Ni and Al powder mixtures," *Combust., Expl., Shock Waves*, **24**, No. 3, 324–330 (1988).
31. L. Thiers, A. S. Mukasyan, and A. Varma, "Thermal explosion in Ni—Al system: influence of reaction medium microstructure," *Combust. Flame*, **131**, Nos. 1–2, 198–209 (2002).
32. Z. Yue, L. Li, J. Zhou, et al., "Preparation and characterization of NiCuZn ferrite nanocrystalline powders by auto-combustion of nitrate-citrate gels," *Mater. Sci. and Eng. B*, **64**, 68–72 (1999).
33. J. McKittrick, L. E. Shea, C. F. Bacalski, and E. J. Bosze, "The influence of processing parameters on luminescent oxides produced by combustion synthesis," *Displays*, **19**, No. 4, 169–172 (1999).
34. A. U. Limaye and J. J. Helble, "Effect of precursor and solvent on morphology of zirconia nanoparticles produced by combustion aerosol synthesis," *J. Amer. Ceram. Soc.*, **86**, No. 2, 273–278 (2003).
35. Choong-Hwan Jung, Sahil Jalota, and Sarit B. Bhaduri, "Quantitative effects of fuel on the synthesis of Ni/NiO particles using a microwave-induced solution combustion synthesis in air atmosphere," *Mater. Lett.*, **59**, Nos. 19–20, 2426–2432 (2005).
36. K. H. Wu, C. H. Yu, Y. C. Chang, and D. N. Horng, "Effect of pH on the formation and combustion process of sol-gel auto-combustion derived NiZn ferrite/SiO_2 composites," *J. of Solid State Chem.*, **177**, No. 11, 4119–4125 (2004).
37. K. H. Wu, Y. C. Chang, T. C. Chang, et al., "Effects of SiO_2 content and solution pH in raw materials on Ni—Zn ferrite magnetic properties," *J. of Magnetism and Magnetic Mater.*, **283**, Nos. 2–3, 380–384 (2004).
38. R. D. Purohit, B. P. Sharma, K. T. Pillia, and A. K. Tyagi, "Ultrafine ceria powders via glycine-nitrate combustion," *Mater. Res. Bull.*, **36**, 2711 (2001).
39. T. M. Tillotson, A. E. Gash, R. L. Simpson, et al., "Nanostructured energetic materials using sol-gel methodologies," *J. Non-Crystalline Solids*, **285**, 338–345 (2001).
40. B. J. Clapsaddle, A. E. Gash, J. H. Satcher, and R. L. Simpson, "Silicon oxide in an iron (III) oxide matrix: the sol-gel synthesis and characterization of Fe—Si mixed oxide nanocomposites that contain iron oxide as the major phase," *J. Non-Crystalline Solids*, **331**, 190–201 (2003).
41. P. Dinka and A. Mukasyan, "In situ preparation of the supported catalysts by solution combustion synthesis," *J. Phys. Chem.*, **109**, No. 46, 21627–21633 (2005).
42. A. S. Rogachev, H. E. Grigoryan, and D. Yu. Kovalev, "Combustion synthesis and structure formation in the sol-gel systems," *Indo-Russian Workshop on Self-Propagating High Temperature Synthesis*, November 27–27, 2008, Bangalore, India, Abstracts, pp. IL–02.
43. S. Sharma and M. S. Hegde, "Single step direct coating of 3-way catalysts on cordierite monolith by solution combustion method: high catalytic activity of $Ce_{0.98}Pd_{0.02}O_{2-\delta}$," *Catal. Lett.*, **112**, 69–75 (2006).
44. A. S. Mukasyan and P. Dinka, "Novel method for synthesis of nano-materials: combustion of active impregnated layer," *J. Adv. Eng. Mater.*, **9**, 653–657 (2007).
45. T. F. Grigorieva, A. P. Barinova, and N. Z. Lyakhov, "Mechanochemical synthesis of intermetallic compounds," *Usp. Khimii*, **70**, No. 1, 52–71 (2001).
46. T. Grigorieva, M. Korchagin, and N. Lyakhov, "Combination of SHS and mechanochemical synthesis for nanopowder technologies," *KONA Powder and Particle*, No. 20, 144–158 (2002).
47. F. Bernard and E. Gaffet, "Mechanical alloying in the SHS research," *Intern. J. Self-Propagating High Temperature Synthesis*, **10**, No. 2, 109–132 (2001).
48. Ch. P. Pool and F. G. Owens, *Introduction in Nanotechnology*, John Wiley and Sons, Hoboken, New Jersey (2003).
49. A. I. Gusev, *Nanomaterials, Nanostructures, and Nanotechnologies* [in Russian], Fizmatlit, Moscow (2005).
50. F. Maglia, U. Anselmi-Tamburini, C. Deidda, et al., "Role of mechanical activation in SHS synthesis of TiC," *J. Mater. Sci.*, **39**, 5227–5230 (2004).

51. F. Maglia, C. Milanese, and U. Anselmi-Tamburini, "Combustion synthesis of mechanically activated powders in the Nb—Si system," *J. Mater. Res.*, **17**, No. 8, 1992–1999 (2002).
52. F. Maglia, C. Milanese, U. Anselmi-Tamburini, et al., "Combustion synthesis of mechanically activated powders in the Ta—Si system," *J. Alloys and Compounds*, **385**, 269–275 (2004).
53. F. Maglia, U. Anselmi-Tamburini, C. Cocco, et al., "Combustion synthesis of mechanically activated powders in the Ti—Si system," *J. Mater. Res.*, **16**, No. 4, 1074–1082 (2001).
54. Yang Yun, Lin Zhi-Ming, and Li Jiang-Tao, "Synthesis of SiC by silicon and carbon combustion in air," *J. Europ. Ceram. Soc.*, **29**, 175–180 (2009).
55. M. A. Korchagin and N. Z. Lyakhov, "Self-propagating high-temperature synthesis in mechanically activated compositions," *Khim. Fiz.*, **27**, No. 1, 73–78 (2008).
56. M. A. Korchagin and D. V. Dudina, "Application of self-propagating high-temperature synthesis and mechanical activation for obtaining nanocomposites," *Combust., Expl., Shock Waves*, **43**, No. 2, 176–187 (2007).
57. M. A. Korchagin, T. F. Grigorieva, A. P. Barinova, and N. Z. Lyakhov, "The effect of mechanical treatment on the rate and limits of combustion in SHS processes," *Intern. J. Self-Propagating High Temperature Synthesis*, **9**, No. 3, 307–320 (2000).
58. N. F. Shkodich, N. A. Kochetov, A. S. Rogachev, et al., "Effect of mechanical activation on SHS compositions Ni—Al and Ti—Al," *Izv. Vyssh. Uch. Zaved., Tsvetnaya Metallurgiya*, No. 5, 44–50 (2006).
59. M. Zakeri, R. Yazdani-Rad, M. H. Enayati, and M. R. Rahimipour, "Synthesis of nanocrystalline $MoSi_2$ by mechanical alloying," *J. Alloys and Compounds*, **403**, 258–261 (2005).
60. U. Anselmi-Tamburini, F. Maglia, S. Doppiu, et al., "Ignition mechanism of mechanically activated Me—Si (Me═Ti, Nb, Mo) mixtures," *J. Mater. Res.*, **19**, No. 5, 1558–1566 (2005).
61. D. P. Riley, E. H. Kisi, and D. Phelan, "SHS of Ti_3SiC_2: ignition temperature depression by mechanical activation," *J. Europ. Ceram. Soc.*, **26**, 1051–1058 (2006).
62. K. Yang, Y. Yang, Z.-M. Lin, et al., "Mechanical-activation-assisted combustion synthesis of SiC powders with tetrapolifluoroethylene as promoter," *Mater. Res. Bull.*, **42**, 1625–1632 (2007).
63. G. Liu, K. Yang, J. Li, et al., "Combustion synthesis of nanosized β-SiC powder on a large scale," *J. Phys. Chem. C*, **112**, 6285–6292 (2008).
64. Ch. Gras, N. Zink, F. Bernard, and E. Gaffet, "Assisted self-sustaining combustion reaction in the Fe—Si system: mechanical and chemical activation," *Mater. Sci. and Eng. A*, **456**, 270–277 (2007).
65. E. M. Heian, S. K. Khalsa, J. W. Lee,and Z. A. Munir, "Synthesis of dense, high-defect-concentration B_4C through mechanical activation and field-assisted combustion," *J. Amer. Ceram. Soc.*, **87**, No. 5, 779–783 (2004).
66. G. Ji, D. Goran, F. Bernard, et al., "Structure and composition heterogeneity of a FeAl alloy prepared by one-step synthesis and consolidation processing and their influence on grain size characterization," *J. Alloys and Compounds*, **420**, 158–164 (2006).
67. I. C. Atias Adrian, G. A. Ortigoza Villalba, F. A. Deorsola, and B. DeBenedetti, "Synthesis of Mg_2Ni nanostructured by MASHS technique," *J. Alloys and Compounds*, **466**, 205–207 (2008).
68. A. M. Locci, R. Orrù, G. Cao, and Z. A. Munir, "Effect of ball milling on simultaneous spark plasma synthesis and densification of TiC—TiB_2 composites," *Mater. Sci. and Eng. A*, **434**, 23–29 (2006).
69. G. Cabouro, S. Chevalier, E. Gaffet, et al., "Reactive sintering of molybdenum disilicide by spark plasma sinthering from mechanically activated powder mixtures: processing parameters and properties," *J. Alloys and Compounds*, **465**, 344–355 (2008).
70. F. Neves, I. Martins, J. B. Correira, et al., "Reactive extrusion synthesis of mechanically activated Ti—50Ni powders," *Intermetallics*, **15**, 1623–1631 (2007).
71. B. S. B. Reddy, Das Karabi, Das Siddhartha, "A review on the synthesis of in situ aluminum based composites by thermal, mechanical and mechanical-thermal activation of chemical reactions," *J. Mater. Sci.*, **42**, 9366–9378 (2007).
72. M. Schoenitz, T. Ward, and E. L. Dreizin, "Preparation of energetic metastable nano-composite materials by arrested reactive milling," *Mater. Res. Soc. Symp. Proc.*, **800**, A2.6.1 (2004).
73. B. S. B. Reddy, K. Rajasekhar, M. Venu, et al., "Mechanical activation — assisted solid-state combustion synthesis of in situ aluminum matrix hybrid (Al_3Ni/Al_3O_2) nanocomposites," *J. Alloys and Compounds*, **465**, 97–105 (2008).
74. M. Schoenitz, T. S. Ward, and E. L. Dreizin, "Fully dense nano-composite energetic powders prepared by arrested reactive milling," *Proc. Combust. Inst.*, **30**, 2071–2078 (2005).
75. S. M. Umbrajkar, M. Schoenitz, and E. L. Dreizin, "Control of structural refinement and composition in Al—MoO_3 nanocomposites prepared by arrested reactive milling," *Propellants, Explosives, Pyrotechnics*, **31**, No. 5, 382–389 (2006).
76. S. M. Umbrajkar, Seshadri, M. Schoenitz, et al., "Aluminum-rich Al—MoO_3 nanocomposite powders prepared by arrested reactive milling," *J. Propulsion and Power*, **24**, No. 2, 192–198 (2008).

77. E. I. Maksimov, A. G. Merzhanov, and V. M. Shkiro, "On self-ignition of thermite compositions," *Zh. Fiz. Khimii*, **40**, No. 2, 468–470 (1966).
78. H.-B. Jin, Y. Yang, Y.-X. Chen, et al., "Mechanochemical-activation-assisted combustion synthesis of α-Si_3N_4," *J. Amer. Ceram. Soc.*, **89**, No. 3, 1099–1102 (2006).
79. Y.-X. Chen, J.-T. Li, and J.-S. Du, "Cost effective combustion synthesis of silicon nitride," *Mater. Res. Bull.*, **43**, 1598–1606 (2008).
80. K. Aoyagi, T. Hiraki, R. Sivakumar, et al., "A new route to synthesize β-$Si_{6-z}Al_zO_zN_{8-z}$ powders," *J. Alloys and Compounds*, **441**, 236–240 (2007).
81. R. Sivakumar, K. Aoyagri, and T. Akiyama, "Effect of mechanically activated raw materials on β-sialon formation by combustion synthesis," *J. Mater. Res.*, **22**, No. 10, 2863–2867 (2007).
82. G. Liu, K. Chen, H. Zhou, et al., "Mechanical-activation assisted combustion synthesis of α-SiAlON in air," *Mater. Res. Bull.*, **42**, 989–995 (2007).
83. V. I. Itin, O. G. Terekhova, N. G. Kasatskii, et al., "High-temperature synthesis of TiN with mechanical activation of titanium in nitrogen," *Neorg. Mater.*, **41**, No. 11, 1315–1319 (2005).
84. J. M. Córdoba, M. D. Alcala, M. A. Avilés, M. J. Sayagués, and F. J. Gotor, "New production of TiC_xN_{1-x}-based cermets by one-step mechanically induced self-sustaining reaction: powder synthesis and pressureless sintering," *J. Europ. Ceram. Soc.*, **28**, 2085–2098 (2008).
85. S. L. Birks and H. Friedman, "Particle size determination from X-ray line broadening," *J. Appl. Phys.*, **17**, 687–692 (1946).
86. G. K. Williamson and W. H. Hall, "X-ray line broadening from filed aluminum and wolfram," *Acta Metallurgica*, **1**, 22–31 (1953).
87. C. E. Wen, K. Kobayashi, A. Sugiyama, T. Nishio, and A. Matsumoto, "Synthesis of nanocrystallite by mechanical alloying and in situ observation of their combustion phase transformation in Al_3Ti," *J. Mater. Sci.*, **35**, 2099–2105 (2000).
88. Y. Shoshin, R. Mudryy, and E. Dreizin, "Preparation and characterization of energetic Al—Mg mechanical alloy powders," *Combust. Flame*, **128**, 259–269 (2002).
89. M. Schoenitz, E. Dreizin, and E. Shtessel, "Constant volume explosions of aerosols of metallic mechanical alloys and powder blends," *J. Propulsion Power*, **19**, No. 3, 405–412 (2003).
90. Y. Shoshin and E. Dreizin, "Laminar lifted flame speed measurements for aerosols of metals and mechanical alloys," *AIAA J.*, **42**, No. 7, 1416–1426 (2004).
91. M. Schoenitz, X. Zhu, and E. L. Dreizin, "Mechanical alloys in the Al-rich part of the Al—Ti binary system," *J. Metast. Nanocryst. Mater.*, **20–21**, 455–461 (2004).
92. V. K. Smolyakov, "Combustion of mechanically activated heterogeneous systems," *Combust., Expl., Shock Waves*, **41**, No. 3, 319–325 (2005).
93. L. G. Abdulkarimova, T. A. Ketegenov, Z. A. Mansurov, et al., "Effect of phase transformation on nonisothermal synthesis in mechanically activated heterogeneous systems," *Combust., Expl., Shock Waves*, **45**, No. 1, 48–58 (2009).
94. A. S. Rogachev, N. A. Kochetov, V. V. Kurbatkina, et al., "Microstructural aspects of gasless combustion of mechanically activated mixtures. I. High-speed microvideorecording of the Ni + Al composition," *Combust., Expl., Shock Waves*, **42**, No. 4, 421–429 (2006).
95. A. S. Rogachev, "Waves of exothermal reactions in multilayer nanofilms," *Usp. Khimii*, **77**, No. 1, 22–38 (2008).
96. T. W. Barbee and T. Weihs, "Ignitable heterogeneous stratified structure for the propagating of an internal exothermic chemical reaction along an expanding wavefront and method of making same," US Pat. 5538795, July 23, 1996.
97. A. G. Merzhanov and A. S. Mukasyan, *Solid-State Combustion* [in Russian], Torus Press, Moscow (2007).
98. A. J. Gavens, D. Van Heerden, A. B. Mann, et al., "Effect of intermixing on self-propagating exothermic reactions in Al/Ni nanolaminate foils," *J. Appl. Phys.*, **87**, No. 3, 1255–1263 (2000).
99. A. S. Rogachev, A. E. Grigoryan, E. V. Illarionova, et al., "Gasless combustion of Ti–Al bimetallic multilayer nanofoils," *Combust., Expl., Shock Waves*, **40**, No. 2, 166–171 (2004).
100. Y. N. Picard, D. P. Adams, J. A. Palmer, and S. M. Yalisove, "Pulsed laser ignition of reactive multilayer films," *Appl. Phys. Lett.*, **88**, 144102(1–3) (2006).
101. D. P. Adams, V. C. Hodges, M. M. Bai, et al., "Exothermic reactions in Co/Al nanolaminates," *J. Appl. Phys.*, **104**, 043502(1–7) (2008).
102. L. A. Clevenger, C. V. Tompson, and K. N. Tu, "Explosive silicidation in nickel/amorphous-silicon multilayer thin films," *J. Appl. Phys.*, **67**, No. 6, 2894–2898 (1990).
103. M. E. Reiss, C. M. Esber, D. Van Heerden, et al., "Self-propagating formation reactions in Nb/Si multilayers," *Mater. Sci. and Eng. A*, **261**, 217–222 (1999).
104. K. J. Blobaum, M. E. Reiss, J. M. Plitzko Lawrence, and T. P. Weihs, "Deposition and characterization of a self-propagating CuO_x/Al thermite reaction in a multilayer foil geometry," *J. Appl. Phys.*, **94**, No. 5, 2915–2922 (2003).
105. A. S. Shteinberg, V. A. Shcherbakov, and Z. A. Munir, "Kinetics of combustion in the layered Ni—Al system," *Combust. Sci. and Technol.*, **169**, 1–24 (2001).
106. E. Ma, C. V. Tompson, L. A. Clevenger, and K. N. Tu, "Self-propagating explosive reactions in Al/Ni mul-

tilayer thin films," *Appl. Phys. Lett.*, **57**, No. 12, 1262–1264 (1990).
107. T. S. Dyer and Z. A. Munir, "The synthesis of nickel aluminides by multilayer self-propagating combustion," *Metallurg. and Mater. Trans. B: Process Metallurgy and Mater. Processing Sci.*, **26**, No. 3, 603–610 (1995).
108. V. A. Shcherbakov, A. S. Shteinberg, and Z. A. Munir, "Formation of the final product during combustion of the Ni–Al layered system," *Dokl. Ross. Akad. Nauk*, **364**, No. 5, 647–652 (1999).
109. A. S. Shteinberg and V. A. Knyazik, "Macrokinetics of high-temperature heterogeneous reactions: SHS aspects," *Pure and Appl. Chem.*, **64**, 965–976 (1992).
110. A. S. Shteinberg and V. A. Knyazik, "Electrocombustion," in: *Proc. Zel'dovich Memorial: Combustion, Detonation, Shock Waves*, September 12–17, 1995, pp. 358–372.
111. X. Qiu and J. Wang, "Experimental evidence of two-stage formation of Al_3Ni in reactive Ni/Al multilayer foils," *Scripta Materialia*, **56**, 1055–1058 (2007).
112. A. G. Merzhanov, E. B. Pis'menskaya, V. I. Ponomarev, and A. S. Rogachev, "Dynamic X-ray photography of phase transformations during synthesis of intermetallides in the thermal explosion mode," *Dokl. Ross. Akad. Nauk*, **363**, No. 2, 203–207 (1998).
113. D. P. Adams, M. A. Rodrigues, C. P. Tigges, and P. G. Kotula, "Self-propagating, high-temperature combustion synthesis of rhombohedral AlPt thin films," *J. Mater. Res.*, **21**, 3168–3179 (2006).
114. E. Ma, "Growth of amorphous silicide during Ti/Si interfacial reactions in multilayer thin films," *Mater. Sci. and Eng. A.*, **398**, 60–65 (2005).
115. V. I. Itin and Yu. S. Naiborodenko, *High-Temperature Synthesis of Intermetallic Compounds* [in Russian], Izd. Tomsk. Univ., Tomsk (1989).
116. T. Lehnert, S. Tixier, P. Böni, and R. Gotthardt, "A new fabrication process for Ni—Ti shape memory thin films," *Mater. Sci. and Eng.*, **A273–275**, 713–716 (1999).
117. M. A. Ponomarev, V. A. Shcherbakov, and A. S. Shteinberg, "Specific features of combustion of thin layers of the titanium–boron powder mixture," *Dokl. Ross. Akad. Nauk*, **340**, No. 5, 642–645 (1995).
118. S. T. Vadchenko, I. P. Borovinskaya, and A. G. Merzhanov, "Solid-flame combustion of thin films," *Dokl. Ross. Akad. Nauk*, **408**, No. 2, 211–213 (2006).
119. S. G. Vadchenko, I. P. Borovinskaya, and A. G. Merzhanov, "SHS in thin films. Possibilities of engineering applications," *Izv. Vyssh. Uch. Zaved., Tsvet. Metallurg.*, No. 5, 36–43 (2006).
120. A. P. Aldushin and B. I. Khaikin, "Combustion of mixtures forming condensed reaction products," *Fiz. Goreniya Vzryva*, **10**, No. 3, 313–323 (1974).
121. A. P. Hard and P. V. Phung, "Propagation of gasless reactions in solids. 1. Analytical study of exothermic intermetallic reaction rates," *Combust. Flame*, **21**, No. 1, 77–89 (1973).
122. R. Armstrong, "Models for gasless combustion in layered materials and random media," *Combust. Sci. and Technol.*, **71**, 155–174 (1990).
123. R. Armstrong and M. Koszykowski, in: Z. A. Munir and J. B. Holt (eds.), *Combustion and Plasma Synthesis of High-Temperature Materials*, VCY, New York (1990), p. 88.
124. R. Armstrong, "Theoretical models for the combustion of alloyable materials," *Metallurg. Trans. A*, **23**, No. 9, 2339–2347 (1992).
125. A. B. Mann, A. J. Gavens, M. E. Reiss, et al., "Modeling and characterizing the propagation velocity of exothermic reactions in multilayer foils," *J. Appl. Phys.*, **82**, No. 3, 1178–1188 (1997).
126. E. Ma, C. V. Thompson, and L. A. Clevenger, "Nucleation and growth during reactions in multilayer AI/Ni films: The early stage of Al, Ni formation," *J. Appl. Phys.*, **69**, No. 4, 2211–2218 (1991).
127. S. Jayaraman, O. M. Knio, A. B. Mann, and T. P. Weihs, "Numerical predictions of oscillatory combustion in reactive multilayers," *J. Appl. Phys.*, **86**, No. 2, 800–809 (1999).
128. J. C. Trenkle, J. Wang, T. P. Weihs, and T. C. Hufnagel, "Microstructural study of an oscillatory formation reaction in nanostructured reactive multilayer foils," *Appl. Phys. Lett.*, **87**, 153108(1–3) (2005).
129. A. S. Rogachev, N. A. Kochetov, I. Yu. Yagubova, et al., "Some features of SHS-process in the multilayer Ti/Al foils," *Intern. J. Self-Propagating High-Temperature Synthesis*, **13**, No. 4, 285–291 (2004).
130. S. Jayaraman, A. B. Mann, M. Reiss, et al., "Numerical study of the effect of heat losses on self-propagating reactions in multilayer foils," *Combust. Flame*, **124**, 178–194 (2001).
131. E. Besnoin, S. Cerutti, O. M. Knio, and T. P. Weihs, "Effect of reactant and product melting on self-propagating reactions in multilayer foils," *J. Appl. Phys.*, **92**, No. 9, 5474–5481 (2002).
132. A. Makino, "Heterogeneous flame propagation in the self-propagating high-temperature synthesis (SHS) process in multi-layer foils for three components system: Theory and experimental comparison," *Proc. Combust. Inst.*, **31**, 1813–1820 (2007).
133. K. J. Blobaum, D. Van Heerden, A. J. Gavens, and T. P. Weihs, "Al/Ni formation reactions: characterization of the metastable Al_9Ni_2 phase and analysis of its formation," *Acta Materialia*, **51**, 3871–3884 (2003).

134. J.-C. Gachon, A. S. Rogachev, H. E. Grigoryan, et al., "On the mechanism of heterogeneous reaction and phase formation in the Ti/Al multilayer nanofilms," *Acta Materialia*, **53**, 1225–1231 (2005).